Thiopurines inhibit coronavirus Spike protein processing and incorporation into progeny virions

Eric S. Pringle [1,*], Brett A. Duguay [1,*], Maxwell P. Bui-Marinos [2,3], Rory P. Mulloy [2,3], Shelby L. Landreth [4,5], Krishna Swaroop Desireddy [6], Stacia M. Dolliver [1], Shan Ying [1], Taylor Caddell [1], Patrick D. Slaine [1], Stephen L. Bearne [6,7], Darryl Falzarano [4,5], Jennifer A. Corcoran [2,3], Denys A. Khaperskyy [1,#], Craig McCormick [1,#]

[1]Department of Microbiology & Immunology, Dalhousie University, 5850 College Street, Halifax NS, Canada B3H 4R2

[2]Department of Microbiology, Immunology and Infectious Diseases, University of Calgary, 2500 University Drive NW, Calgary AB, Canada T2N 1N4

[3]Snyder Institute for Chronic Diseases and Charbonneau Institute of Cancer Research, University of Calgary, 2500 University Drive NW, Calgary AB, Canada T2N 1N4

[4]Department of Veterinary Microbiology, Western College of Veterinary Medicine, University of Saskatchewan, 52 Campus Drive, Saskatoon SK, Canada S7N 5E3

[4]Vaccine and Infectious Disease Organization (VIDO), 120 Veterinary Road, Saskatoon SK, Canada S7N 5E3

[5] Department of Biochemistry and Molecular Biology, Dalhousie University, Halifax, NS, Canada B3H 4R2

[6]Department of Chemistry, Dalhousie University, Halifax, NS, B3H 4R2, Canada

*Co-lead authors

[#]Co-corresponding authors: D.A.K., D.Khaperskyy@dal.ca, C.M., craig.mccormick@dal.ca

Running Title: Thiopurines inhibit coronavirus Spike glycoprotein processing

Keywords: virus, coronavirus, SARS-CoV-2, HCoV-229E, HCoV-OC43, thiopurine, 6-thioguanine, 6-thioguanosine, unfolded protein response, glycosylation, Spike, assembly, GTPase, host-targeted antiviral

ABSTRACT

There is an outstanding need for broadly acting antiviral drugs to combat emerging viral diseases. Here, we report that thiopurines inhibit the replication of the betacoronaviruses HCoV-OC43 and SARS-CoV-2, and to a lesser extent, the alphacoronavirus HCoV-229E. 6-Thioguanine (6-TG) disrupted early stages of infection, limiting synthesis of full-length and subgenomic HCoV RNAs. Furthermore, consistent with our previous report on the effects of thiopurines on influenza A virus (IAV) glycoproteins, we observed that 6-TG inhibited accumulation of Spike glycoproteins from diverse HCoVs. Specifically, 6-TG treatment decreased the accumulation of Spike proteins and increased their electrophoretic mobility to match the properties of Spike following enzymatic removal of N-linked oligosaccharides with Peptide:N-glycosidase F (PNGaseF). SARS-CoV-2 virus-like particles (VLPs) harvested from 6-TG-treated cells were deficient in Spike. 6-TG treatment had a similar effect on lentiviruses pseudotyped with SARS-CoV-2 Spike; lentiviruses could be harvested from cell supernatants, but they were deficient in Spike and unable to infect human cells bearing ACE2 receptors. Together, these findings from complementary ectopic expression and infection models strongly indicate that defective Spike trafficking and processing is an outcome of 6-TG treatment. At low micromolar doses, the primary known mode of action of 6-TG is selective inhibition of the small GTPase Rac1. However, we show that selective chemical inhibitors of the small GTPases Rac1, CDC42 and Rho had no effect on Spike processing and accumulation, whereas the broad GTPase agonist ML099 was able to counter the effects of 6-TG, suggesting that an unknown GTPase could be the relevant 6-TG-target protein involved in regulating Spike processing and accumulation. Overall, these findings provide important clues about the mechanism of action of a candidate antiviral that can broadly target HCoVs and suggest that small GTPases may be promising targets for host-targeted antivirals.

57 **INTRODUCTION**

58 Coronaviruses (CoVs) are enveloped viruses with positive-sense, single-stranded RNA
59 ((+)ssRNA) genomes. Seven human CoVs (HCoVs) are divided into two genera, the
60 alphacoronaviruses (HCoV-NL63 and HCoV-229E) and betacoronaviruses (HCoV-OC43, HCoV-
61 HKU1, MERS-CoV, SARS-CoV and SARS-CoV-2). Following entry into host cells, the
62 (+)ssRNA CoV genome is immediately translated into polyproteins that are cleaved by viral
63 cysteine proteases into 16 non-structural proteins (NSPs). These NSPs include the transmembrane
64 nsp3-nsp4-nsp6 complex that generates a complex endoplasmic reticulum (ER)-derived
65 reticulovesicular network that includes replication organelles known as double-membrane vesicles
66 (DMVs) (1–8). In DMVs, the nsp3-nsp4-nsp6 complex provides a physical anchor for the viral
67 replicase-transcriptase complex (RTC) that replicates the large viral genome and synthesizes
68 subgenomic mRNAs (9, 10). These viral RNAs traverse a crown-shaped pore to exit the DMV (8).
69 In the cytoplasm, viral mRNAs are translated into structural proteins; Nucleocapsid (N) is
70 synthesized via free ribosomes in the cytoplasm, whereas mRNAs encoding envelope proteins are
71 translated and processed in the ER and accumulate in the ER-Golgi-intermediate compartment
72 (ERGIC). HCoV assembly takes place when full-length viral genomic RNA coated with N buds
73 into the ERGIC to acquire the viral envelope and associated envelope proteins (11–13). These
74 progeny viruses traverse the Golgi apparatus and *trans*-Golgi network (TGN), where envelope
75 proteins receive additional post-translational modifications, and exit the cell via lysosomal
76 exocytosis (14).

77 CoV envelope proteins are subject to extensive processing in the secretory pathway. The
78 viral envelope proteins Spike, Envelope (E) and Matrix (M) that are found in all HCoVs, as well
79 as Hemagglutinin-Esterase (H-E) found in only HCoV-OC43 and HCoV-HKU1, are synthesized
80 in the ER as transmembrane (TM) proteins (15). CoV Spike proteins are large type I TM proteins
81 that are heavily N-glycosylated, which promotes proper folding, trimerization and trafficking (16).
82 Subsequent proteolytic processing is required to activate these glycosylated Spike trimers,
83 generating the S1 attachment protein and liberating the mature amino-terminal fusion peptide of
84 the S2 fusion protein, both of which are essential components of infectious CoV virions that can
85 enter target cells (17, 18). Proteolytic activation of Spike can occur in the secretory pathway of
86 infected cells or unprocessed Spike can be incorporated into virions and Spike processing can
87 occur during attachment and entry into naïve cells in a process that involves multiple host serine

88 and cysteine proteases. M is the most abundant CoV envelope protein and it serves as a scaffold
89 for viral assembly. It is a multi-spanning membrane protein, with a small lumenal amino-terminus
90 that is N-glycosylated, and three transmembrane domains followed by a large, cytoplasmic
91 carboxy-terminal domain known as the endodomain that governs interactions with the other
92 structural proteins (Spike, E and N), as well as M-M interactions. E is a small type I transmembrane
93 protein that forms pentameric complexes and functions as a viroporin, increasing the lumenal pH
94 in the Golgi and protecting Spike from proteolysis (reviewed in (19)). The viroporin activity may
95 support de-acidification of lysosomes and subsequent lysosomal exocytosis. M and E proteins both
96 govern the intracellular trafficking and processing of Spike (20).

97 The striking remodeling of the ER to create replication organelles, as well as the reliance
98 on the ER for synthesis and processing of viral glycoproteins, has prompted investigations into the
99 effects of HCoV infection on ER stress and the unfolded protein response (UPR). Several
100 coronaviruses (CoVs) have been shown to activate the UPR, including infectious bronchitis virus
101 (IBV) (21, 22), mouse hepatitis virus (MHV) (23), transmissible gastroenteritis virus (TGEV) (24),
102 human coronavirus (HCoV)-OC43 (25) and SARS-CoV (26–28). However, proximal UPR sensor
103 activation does not always elicit downstream UPR transcription responses during CoV replication
104 (29), which suggests complex regulation of the UPR by certain CoVs. Ectopic expression of Spike
105 proteins from MHV (23), HCoV-HKU1 (27) and SARS-CoV (27, 30) have all been shown to be
106 sufficient for UPR activation in cell culture. Additional transmembrane CoV proteins have been
107 shown to be sufficient to induce the UPR, including SARS-CoV non-structural protein 6 (nsp6)
108 (31), ORF3a (32) and ORF8ab (33) proteins. Despite these discoveries, our understanding of the
109 regulation of the UPR in CoV infection remains incomplete, and little is known about UPR
110 regulation in SARS-CoV-2 infection.

111 The emergence of SARS-CoV and MERS-CoV from animal reservoirs, followed by the
112 current SARS-CoV-2 pandemic, has spurred efforts to discover and develop effective antivirals.
113 These efforts have benefitted from drug repurposing strategies to identify antivirals amongst drugs
114 that have already been approved for use in humans. We showed previously that thiopurines 6-
115 thioguanine (6-TG) and 6-thioguanosine (6-TGo) selectively inhibited influenza A virus (IAV)
116 replication by activating the UPR and interfering with the processing and accumulation of viral
117 glycoproteins (34). Thiopurines have been in clinical use for over 50 years to treat inflammatory
118 diseases and cancer and as immunomodulators. They include azathioprine, 6-mercaptopurine (6-

119 MP) and 6-TG. 6-TG is orally bioavailable and on the World Health Organization's List of
120 Essential Medicines. It is used to treat hematological malignancies, including acute lymphoblastic
121 leukemia (AML), acute lymphocytic leukemia (ALL) and chronic myeloid leukemia (CML), with
122 the primary mechanism of action involving conversion into thioguanine deoxynucleotides and
123 incorporation into cellular DNA, which preferentially kills rapidly dividing cancer cells (35, 36).
124 By contrast, the anti-inflammatory effect of sub-cytotoxic doses of 6-TG for treating inflammatory
125 bowel disease (IBD) is thought to be primarily due to inhibition of the small GTPase Rac1 (37,
126 38). This process requires 6-TG to be metabolized by the purine scavenging enzyme hypoxanthine
127 phosphoribosyltransferase 1 (HPRT1) to yield 6-thioguanosine 5'-monophosphate (6-TGMP),
128 which is then converted to 6-thioguanosine 5'-triphosphate (6-TGTP). 6-TGTP is the active form
129 of the molecule that has been shown to covalently modify a reactive cysteine in the p-loop of Rac1;
130 subsequent hydrolysis of the GTPase-bound 6-TGTP adduct yields a trapped, inactive Rac1-6-
131 TGDP product (37). These host-targeted properties of 6-TG, combined with our knowledge of how
132 6-TG inhibits IAV glycoprotein processing, motivated us to investigate whether 6-TG and related
133 thiopurines might similarly interfere with CoV glycoproteins. Moreover, we reasoned that this
134 kind of host-targeted antiviral activity might act synergistically with the previously reported direct-
135 acting antiviral activity of 6-TG as an inhibitor of MERS-CoV, SARS-CoV and SARS-CoV-2
136 papain-like cysteine proteases PL^{pro} *in vitro* (39–42). Using ectopic expression and cell culture
137 infection models, we discovered that 6-TG and 6-TGo inhibited replication of several CoVs
138 including SARS-CoV-2, which correlated with disruption of Spike processing, as well as Spike
139 accumulation and incorporation into progeny virions. Accumulation of viral subgenomic RNAs
140 and full-length genomes was also inhibited by these thiopurines. Finally, we were able to link the
141 antiviral mechanism of action to the primary known mode of action of 6-TG and related molecules
142 as selective inhibitors of small GTPases (37, 43, 44), which could be overcome by treating with a
143 pan-GTPase agonist. Our findings extend the understanding of the mechanism of action of these
144 candidate host-targeted antivirals and provide a means to study the impact of glycoprotein
145 maturation on coronavirus biology.

146

147

148

149 **RESULTS**

150 **6-Thioguanine and 6-thioguanosine inhibit HCoV replication**. We tested the effects of three
151 thiopurines on SARS-CoV-2 replication in Calu-3 lung adenocarcinoma cells. Treatment with 6-
152 TG, the ribonucleoside 6-TGo, or the related thiopurine 6-MP, caused a striking 4-log decrease
153 in the release of infectious virions after 48 h of infection, with little effect on cell viability
154 [Selectivity Index (SI) 6-TG > 87.0, 6-TGo > 37.4, 6-MP >35.4] (**Figs. 1A, 1B, 1C**). The sub-
155 micromolar EC_{50} values that we observed for all three thiopurines in the Calu-3 infection model
156 were consistent with previously reported values from other groups (42, 45). 6-TG was well
157 tolerated in three other cell lines we used for HCoV infection models (HCT-8, Huh7.5, and
158 primary hTERT-immortalized fibroblasts) (Fig 1D). We tested the ability of 6-TG to inhibit the
159 betacoronavirus HCoV-OC43 and the alphacoronavirus HCoV-229E and found that low
160 micromolar doses of the ribonucleoside 6-TGo had similar inhibitory effects against HCoV-229E
161 and HCoV-OC43 in their respective infection models, whereas 6-MP had no effect **(Figs. 1E,**
162 **1F)**. Because UPR stimulators thapsigargin (Tg) and tunicamycin (TM) inhibit coronavirus
163 replication (46–49) and our previous work demonstrated that 6-TG can inhibit glycosylation of
164 influenza A virus (IAV) glycoproteins and stimulate ER stress (34), we included TM as a
165 positive control in these studies. In hTert-BJ cells, 6-TG inhibited HCoV-OC43 replication at
166 low micromolar doses, consistent with our observations in the HCT-8 cell infection model;
167 however, HCoV-229E replication in hTert-BJ cells was minimally affected across a range of
168 sub-cytotoxic concentrations (**Figs. 1G, 1H**). Together, these findings suggested that 6-TG was
169 more effective at inhibiting HCoV-OC43 and SARS-CoV-2 replication than HCoV-229E, and
170 that this differential susceptibility can be at least partly attributed to differences between these
171 viruses.

172

173 **6-Thioguanine impedes viral genome replication and subgenomic RNA synthesis.** Next, we
174 investigated which stages of virus replication were affected by 6-TG treatment. We performed
175 multi-round HCoV-OC43 infections of HEK293T cells at an MOI of 0.1. Infected cells were
176 treated with 10 μM 6-TG or DMSO immediately after infection, and cell lysates and
177 supernatants were harvested at regular intervals for the next 48 hours. 6-TG treatment caused a
178 ~40-fold reduction in infection during the first day of infection. Virion release from control cells

179 plateaued at 24 hours post-infection, whereas peak release of infectious virions from 6-TG-
180 treated cells occurred much later at 48 hours post-infection **(Fig. 2A)**. Similarly, measuring viral
181 particle release by RT-qPCR amplification of viral genomes revealed a ~20-fold reduction in
182 virus titer **(Fig. 2B)** throughout the first day of infection. Next, we investigated the ability of 6-
183 TG to disrupt viral RNA synthesis. Putative full-length RNA, as detected by primers targeting
184 *ORF1a*, was reduced by ~10-fold throughout most stages of infection. Similar decreases were
185 detected using primers targeting the coding region of *Spike* and *N* genes after 6 h post-infection,
186 with much larger 40-fold differences at 6 h post-infection **(Fig. 2C)**. These disruptions in viral
187 RNA accumulation correlated with changes in the localization of N, the viral nucleoprotein.
188 Immunostaining HCoV-OC43 infected cells with an anti-N antibody revealed a punctate staining
189 pattern at 6 hours post-infection **(Fig. 2D)**. By 24 h post-infection, N immunostaining was less
190 punctate and more peripheral as at later stages of infection. The N immunostaining was markedly
191 altered in 6-TG-treated infected cells, with brighter punctate staining patterns at 6 hours post-
192 infection and large puncta still visible at 24 h post-infection. The formation of replication
193 compartments was also delayed in 6-TG treated cells, as determined by immunostaining for
194 dsRNA **(Fig. 2E)**; specifically, we observed dsRNA signal at 6 hpi, which correlated with
195 decreased viral RNA detected by RT-qPCR **(Fig. 2C)**. Together, these findings indicate that 6-
196 TG reduces the synthesis of viral RNAs required to support efficient HCoV replication.

197 In our recent study, the antiviral mechanism of action of 6-TG and 6-TGo against IAVs
198 involved activation of the UPR and interference with the processing and accumulation of viral
199 glycoproteins. In these experiments, IAV infection of vehicle-treated A549 cells revealed very
200 little detectable UPR late in infection at 24 h post-infection, whereas 6-TG stimulated all three
201 arms of the UPR, with transactivation of XBP1s target gene *ERdj4*, ATF6-N target genes *BiP* and
202 *HERPUD1* and ATF4 target gene *CHOP* (34). Thus, thiopurines markedly altered the ER
203 proteostasis landscape to the detriment of IAV replication. By contrast, many HCoVs have been
204 shown to activate the UPR, including infectious bronchitis virus (IBV) (21, 22), mouse hepatitis
205 virus (MHV) (23), transmissible gastroenteritis virus (TGEV) (24), human coronavirus (HCoV)-
206 OC43 (25) and SARS-CoV (26–28). Here, HCoV-OC43 infection caused induction of *Xbp1*
207 transcript, potent accumulation of spliced *Xbp1*, and transactivation of XBP1s target genes *ERdj4*
208 and *Edem1*, providing strong evidence for activation of the IRE1 arms of the UPR **(Figs. S1A,**
209 **S1B)**. Regulation of the PERK/ATF4 arm of the UPR may be more complex, as HCoV-OC43

210 infection caused accumulation of *ATF3* mRNA but no change in *CHOP*, even though they are both
211 encoded by ATF4 target genes. Similarly, we observed increased expression of ATF6-N target
212 genes *HERPUD1* and *Xbp1* but no increases in BiP mRNA or protein **(Figs. S1A, S1B)**. Thus,
213 HCoV-OC43 interactions with the UPR appear to be complex and marked by strong stimulation
214 of IRE1, which is consistent with observations from others (25). In marked contrast to our IAV
215 studies, 6-TG treatment generally delayed or suppressed the downstream UPR transcriptional
216 response **(Fig. S1A)**, which could be attributed to 6-TG-mediated delays in viral replication and
217 the accumulation of viral RNAs and proteins **(Fig. 2)**. Finally, it should be noted that UPR
218 transcripts accumulated to high levels in vehicle-treated cells despite the fact that HCoV-OC43,
219 like all HCoVs, has mechanisms to potently shut off host antiviral gene expression (25). Using
220 ribopuromycinylation assays, we demonstrated that HCoV-OC43 greatly reduced translation of
221 host mRNAs at the expense of viral mRNAs encoding a few abundant viral proteins **(Fig. S1C,**
222 **lane 4)**. 6-TG treatment had no effect on global rates of translation initiation in HCoV-OC43
223 infected cells, with the only changes evident being the apparent loss of some abundant viral
224 proteins **(Fig. S1C, lane 6)**. Together, these observations suggested that 6-TG inhibition of HCoV-
225 OC43 infection limits the strong activation of IRE1 and accumulation of XBP1s target genes, and
226 that even though 6-TG interferes with synthesis of viral full-length genomic RNAs and
227 subgenomic RNAs, host shutoff is unperturbed.

228

229 **6-Thioguanine inhibits Spike processing and accumulation.** We previously reported that 6-TG
230 and 6-TGo inhibited the processing and accumulation of IAV glycoproteins hemagglutinin (HA)
231 and neuraminidase (NA) (34). Here, we observed a similar defect in SARS-CoV-2 infected cells;
232 lysates harvested from SARS-CoV-2-infected Calu-3 cells at 48 h post-infection showed a sharp
233 decrease in all four structural proteins following 6-TG treatment **(Fig. 3A)**, consistent with a sub-
234 micromolar EC50 discussed above **(Fig. 1B)**. Treatment of SARS-CoV-2-infected Huh-7.5 cells
235 with 10 μM 6-TG also reduced the accumulation of viral structural proteins, which was especially
236 evident for Spike **(Fig. 3B)**. These findings led us to further investigate the effects of 6-TG on
237 SARS-CoV-2 structural protein expression. Transfection of HEK293T cells with each SARS-
238 CoV-2 structural protein independently revealed that 6-TG had no effect on E or N accumulation,
239 whereas Spike processing was noticeably inhibited (**Fig. 3C**). We also observed that 6-TG

240 treatment caused a loss of a slow-migrating species of M **(Fig. 3C)**, which likely represented the
241 glycosylated form of the protein that has been previously reported for other HCoVs (50). Thus, it
242 appears that amongst the SARS-CoV-2 structural proteins, only the glycosylated Spike and M
243 proteins are altered when they are expressed independently in HEK293T cells.

244 To further explore the effects of 6-TG on Spike, we ectopically expressed Spike, then
245 treated the cells with a range of sub-cytotoxic 6-TG concentrations before harvesting lysates and
246 processing for immunoblotting **(Figs. 3D, 3E)**. Spike appeared as two bands when immunoblots
247 are probed with an anti-S1 receptor binding domain (RBD) antibody, a high-molecular weight
248 (MW) precursor S0 band (~203 kDa) and a lower molecular weight band representing the protease-
249 cleaved S1 attachment protein (~96 kDa). Increasing concentrations of 6-TG once again led to the
250 accumulation of a prominent single band at an unexpected MW (~137 kDa) **(Fig. 3D)**. Because 6-
251 TG treatment caused Spike to migrate faster during SDS-PAGE than expected, we hypothesized
252 that the lower MW species could arise from a glycosylation defect. We treated lysates from Spike-
253 expressing HEK293T cells with Peptide-*N*-Glycosidase F (PNGase F), an amidase that cleaves the
254 bond between N-acetylglucosamine (GlcNAc) and asparagine, effectively removing all N-linked
255 glycans from the polypeptide chain (unless the core GlcNAc is modified by α-1,3-fucose) (51).
256 PNGase F treatment caused Spike from the DMSO-treated cells to migrate similarly to Spike from
257 6-TG-treated cells **(Fig. 3F)**. We confirmed the identity of the high MW Spike band as the
258 uncleaved S0 precursor protein by generating and testing a mutant Spike protein in which the basic
259 residues in the furin cleavage site joining S1 and S2 were substituted by alanines, yielding a
260 protease cleavage-resistant Spike protein. Cells transfected with this S0 construct and treated with
261 6-TG prior to lysis revealed that the S0 construct was also sensitive to PNGaseF treatment; the 6-
262 TG/PNGaseF-treated S0 migrated similarly to 6-TG/PNGaseF-treated WT Spike by SDS-PAGE.
263 Several studies have mapped O-linked glycans on SARS-CoV-2 Spike (52–54); these
264 modifications appear to follow the "O-follow-N rule" whereby N-glycosylation is followed by O-
265 glycosylation on nearby residues (52). Thus, the apparent differences in molecular weight between
266 vehicle/PNGaseF-treated Spike and 6-TG/PNGaseF-treated Spike could stem from residual O-
267 linked glycans on Spike that are absent in the 6-TG-treated proteins. These findings were
268 corroborated using carboxy-terminal FLAG-tagged Spike proteins from SARS-CoV-2 and MERS-
269 CoV that also displayed a fast-migrating, under-glycosylated S0 species and loss of the S2 subunit

270 following 6-TG treatment **(Fig. 3G)**. Taken together, these results suggest that 6-TG inhibits
271 normal glycosylation and processing of Spike.

272 A failure of Spike to migrate from the ER to the Golgi could inhibit glycan maturation and
273 cleavage by furin. In our previous work, we observed that 6-TG treatment did not reduce levels of
274 Class I HLA proteins at the cell surface (34), which we interpreted as evidence that 6-TG did not
275 globally affect processing and secretion of host cell glycoproteins. Here, we tested the role of 6-
276 TG on the secretory pathway by using a *Gaussia* luciferase assay, which is secreted from cells by
277 way of a native secretion signal (55). As a control we used the Arf1-inhibitor Brefeldin A (BFA)
278 which potently inhibits protein trafficking from the ER to the Golgi (56, 57). BFA is toxic to cells
279 at micromolar doses, but we could still detect secretory pathway inhibition at 250 nM for 20 h
280 without overt cytotoxicity **(Figs. S2A, S2B)**. A short-term, 6 h treatment with 6-TG (10 μM) had
281 little effect on *Gaussia* luciferase secretion, whereas treatment with BFA (10 μM) greatly
282 decreased secretion. We tested a longer 20 h treatment of 6-TG where we co-transfected Firefly
283 luciferase (Luc2) with *Gaussia* luciferase to help control for the inhibitory effects of 6-TG on
284 HEK293T cell proliferation. This extended 6-TG treatment caused a slight loss of detectable
285 *Gaussia* luciferase activity in the cell supernatant, but once again low-dose treatment of BFA
286 greatly inhibited secretion and increased intracellular retention of *Gaussia* luciferase (Fig. S3C)
287 These experiments strongly corroborated our prior observations that 6-TG treatment does not
288 globally disrupt the secretory pathway. Because of our previous observations of 6-TG-mediated
289 defects in Spike glycosylation, processing and trafficking, we decided to test whether low-dose,
290 long-term treatment with BFA would be sufficient to recapitulate the effects of 6-TG treatment on
291 Spike. However, unlike 6-TG, the secretion inhibitor BFA did not cause any changes in Spike
292 accumulation or processing, as indicated by identical electrophoretic mobility of Spike on
293 immunoblots compared to vehicle control **(Fig. S2D).**

294 To directly monitor Spike protein secretion, we used flow cytometry and surface staining
295 of unpermeablized HEK293T cells transfected with Spike. We co-transfected cells with an EGFP
296 plasmid and gated on EGFP+ cells to measure changes in Spike accumulation. 6-TG reduced
297 surface expression of Spike by ~50% resulting in fewer Spike-positive cells and reduced mean
298 fluorescence intensity. In these experiments, we also tested a Spike protein in which the 19 C-
299 terminal residues were removed (Spike-Δ19); this widely used strategy removes an ER-retrieval
300 signal and enhances incorporation into lentivirus particles (58–60). We found a similar ~50%

301 reduction in trafficking and surface expression of Spike-Δ19 **(Fig. S2E)**. Together, these
302 experiments indicate that 6TG inhibits normal trafficking of Spike to the cell surface but does not
303 broadly inhibit secretion.

304

305 **6-Thioguanine causes a coronavirus assembly defect.** It has been shown that co-transfection of
306 all four SARS-CoV-2 structural proteins allows secretion of virus-like particles (VLPs) (20),
307 which is concordant with earlier studies of other CoV structural proteins (61). However, we
308 observed that when Spike, E, M and N expression vectors were co-transfected into cells, 6-TG
309 treatment not only altered the accumulation and processing of Spike, but also dramatically reduced
310 accumulation of E and M proteins (**Fig. 4A**). Cell supernatants were collected, filtered and pelleted
311 in a sucrose cushion to isolate VLPs, which were then characterized by immunoblotting. We
312 observed a dramatic reduction in VLP production from 6-TG-treated HEK293T cells, and these
313 residual VLPs completely lacked Spike (**Fig. 4B**). These findings indicate that 6-TG not only
314 prevents Spike processing and accumulation, but also its incorporation into VLPs. We then co-
315 transfected cells again with Spike, E, M, and N but omitted structural proteins individually to better
316 understand mechanisms of defective assembly. Our main conclusions are: 1) 6-TG treatment of
317 cells expressing all structural proteins causes a strong Spike-dependent decrease in E expression,
318 2) M resists the Spike glycosylation defect caused by 6-TG, and 3) N enhances expression of E
319 **(Fig 4C)**. To determine if Spike from 6-TG treated cells was still functional, we employed a
320 lentivirus pseudotyping method using Spike-Δ19, which is widely used to measure the neutralizing
321 antibodies to SARS-CoV-2 (58, 62, 63). We performed immunoblots on pseudotyped viruses
322 (PVs) recovered from three independent preparations that we purified by ultracentrifugation
323 through a 20% sucrose cushion. Unlike our previous immunoblots of ectopically expressed Spike
324 from transfected cells, we observed that most of the Spike proteins incorporated into the PVs were
325 fully cleaved into the prominent S1 band **(Fig. 4D)**. However, 6-TG treatment led to a dramatic
326 loss of Spike S0 and S1 species from the purified PVs, compared to little effect on HIV p24 levels
327 in PV cores. We quantified PV yield from these cells by amplifying lentiviral genomes via RT-
328 qPCR from filtered, unconcentrated cell supernatants. 6-TG treatment did not significantly reduce
329 the quantity of capsid-protected genomes released from cells compared to vehicle control **(Fig.
330 4E)**. To determine the effects of 6-TG on PV infectivity, we used purified PVs to infect HEK293A
331 cells that stably express the ACE2 receptor and measured luciferase production in the recipient

332 cells as a measure of successful lentiviral infection. Consistent with deficient Spike incorporation
333 into PVs, we observed that 6-TG treatment reduced PV infectivity by over 50-fold compared to
334 PVs derived from vehicle-treated cells **(Fig. 4F)**. By contrast, PVs derived from vehicle control-
335 and 6-TG-treated cells were equally competent to infect ACE2-deficient HEK293A cells at low
336 levels. This suggests that 6-TG treatment not only inhibits Spike glycosylation and processing, but
337 it also inhibits Spike trafficking and incorporation into lentiviral particles. We next investigated
338 whether these 6-TG-mediated assembly defects altered the morphology of HCoV particles. We
339 concentrated supernatant from HCoV-OC43 infected 293A cells by ultracentrifugation and imaged
340 virions by transmission electron microscopy using negative staining. We observed fewer viral
341 particles in the 6-TG treated samples, and while these particles were of similar size, we noted fewer
342 particles with clearly discernible Spikes **(Fig. 4G)**. Taken together, the strong effects of 6-TG on
343 Spike in transient transfections, heterologous lentivirus infections, and authentic HCoV infections,
344 provide evidence for an additional antiviral mode of action for 6-TG beyond PLpro inhibition or
345 defects in viral RNA synthesis.

346

347 **6-Thioguanine must be processed by HPRT1 to inhibit Spike processing and coronavirus**
348 **replication.**

349 We observed comparable antiviral activities of 6-TG and its ribose-conjugated analogue 6-TGo
350 throughout these studies. Metabolism of 6-TG is initiated by the purine scavenging enzyme
351 hypoxanthine phosphoribosyltransferase 1 (HPRT1) to yield 6-thioguanosine 5'-monophosphate
352 (6-TGMP) **(Fig. 5A)**. 6-TGMP can then be converted to 6-thioguanosine 5'-triphosphate (6-
353 TGTP), the active form of the molecule that has been shown to form a covalent bond with a
354 reactive cysteine in the p-loop of Rac1; subsequent hydrolysis of Rac1-6-TGTP to a diphosphate
355 form renders the GTPase inactive (37). Considering this information, we next sought to determine
356 whether conversion of 6-TG to a ribonucleoside was required for its antiviral activity. First, we
357 synthesized N9-methyl 6-thioguanine (6-TGMe), which prevents conjugation to a ribose sugar due
358 to the methyl group at N9 of the urine ring **(Fig. 5A)**. 6-TGMe displayed low cytotoxicity and no
359 antiviral activity against HCoV-OC43 across a broad range of concentrations **(Fig. 5B)**. Likewise,
360 6-TGMe had no effect on SARS-CoV-2 Spike processing across a range of concentrations between
361 5 μM and 20 μM **(Fig. 5C)**. To corroborate this finding, we used RNA interference to silence

362 expression of *HPRT1* in 293T cells prior to infection with HCoV-OC43 and treatment with 6-TG
363 or vehicle control. RT-qPCR confirmed effective silencing of *HPRT1*(**Fig. 5D**), which had no
364 effect on HCoV-OC43 infection in vehicle control-treated cells **(Fig. 5E)**. By contrast, *HPRT1*
365 silencing significantly restored viral replication in the presence of 6-TG, although replication did
366 not return to the levels in control cells. Together, these findings indicate that 6-TG is a pro-drug
367 that must be metabolized by HPRT1 to convert it to an active form.

368

369 **6-Thioguanine inhibits Spike maturation by inhibiting an unidentified cellular GTPase.** 6-
370 TG inhibits several different GTPases including Rac1, RhoA, and Cdc42 (37, 43, 44). This mode
371 of action was previously shown to inhibit rotavirus replication at sub-micromolar concentrations
372 (64). Here, we sought to determine if any of the known targets of 6-TG were responsible for defects
373 in Spike maturation. We tested known inhibitors of Rac1 (Rac1 Inhibitor V), RhoA (Rhosin), and
374 Cdc42 (CASIN) for cytotoxic effects in HEK293T cells after 24 h incubation using an alamarBlue
375 assay to identify optimal sub-cytotoxic doses for further testing (**Figs. 6A, 6B)**. We also tested a
376 GTPase agonist ML099 that can potently activate Rac1, RhoA, and Cdc42, among other GTPases
377 (65). None of the three GTPase inhibitors had any effect on Spike processing or accumulation
378 **(Fig. 6C)**. Because many additional GTPases have redox-sensitive cysteine residues that could
379 interact with 6-TG, we reasoned that 6-TG could affect viral glycoproteins through an as-yet-
380 unidentified GTPase. In support of this notion, we observed that the broadly acting small GTPase
381 agonist ML099 maintained normal Spike processing in the presence of 6-TG **(Fig. 6D)**. Pre-
382 treating the cells with ML099 before addition of 6-TG further enhanced this effect **(Fig. 6E)**. We
383 attempted to rescue HCoV-OC43 titer in both HCT-8 and HEK293A infection models but instead
384 found that ML099 was itself acting as an antiviral agent **(Fig. 6F)**. While this was worth testing,
385 this result was unsurprising as viral infection likely requires specific or unperturbed GTPase
386 function, including frequent cycling between GTP- and GDP-bound forms. Overall, these data
387 suggest that 6-TG inhibits Spike maturation by inhibiting an unidentified cellular GTPase.

388

389
390

391 **DISCUSSION**

392 The reliance of viruses on the host cell biosynthetic and secretory apparatus, combined with the
393 existence of varied and potent host antiviral mechanisms, makes host targeted antivirals (HTAs)
394 useful additions to our armamentarium of direct-acting antivirals (DAAs). By targeting these host
395 cell processes, HTAs may not be so easily subverted by the rapid viral evolution that frequently
396 undermines DAAs. We recently reported that the thiopurines 6-TG and 6-TGo inhibit influenza A
397 virus (IAV) by selectively disrupting the normal processing and accumulation of HA and NA
398 glycoproteins (34). We hypothesized that other enveloped viruses that rapidly produce a burst of
399 viral glycoproteins would also be susceptible to these thiopurines. Here, we reported that the
400 thioguanine 6-TG disrupted the normal processing and accumulation of CoV Spike glycoproteins
401 and inhibited the release of infectious progeny. This drug-induced Spike processing defect
402 disrupted incorporation of SARS-CoV-2 Spike into VLPs or pseudotyped lentiviruses, which
403 subsequently prevented infection of susceptible, ACE2-expressing cells (Fig. 7). We also
404 significantly advanced our understanding of the molecular mechanism of action of these
405 thiopurines, which had previously been shown to inhibit the small GTPase Rac1 by forming a
406 covalent bond with a redox-sensitive cysteine, preventing further guanine nucleotide exchange.
407 We showed that selective chemical inhibitors of the related small GTPases Rac1, CDC42 and Rho
408 had no effect on Spike processing and accumulation, but a broad GTPase agonist was able to
409 counter the effects of 6-TG, suggesting that there are additional, unknown GTPase targets of 6-TG
410 that are required for normal Spike processing and accumulation. Together, these findings suggest
411 that functioning small GTPases are essential for virus replication and that further development of
412 GTPase inhibitors as host-directed antivirals is warranted.

413 We were intrigued by how 6-TG and 6-TGo strongly inhibited processing and
414 accumulation of IAV and CoV glycoproteins, whereas other viral proteins were relatively
415 unperturbed. However, we also observed that these thiopurines had little effect on global host
416 protein synthesis and secretion. Together, these observations suggested that viral glycoproteins
417 may have properties that make them uniquely sensitive to these drugs. Certainly, viral
418 glycoproteins must adhere to temporal or physical constraints that most host glycoproteins do not.
419 All glycoproteins are synthesized, folded and post-translationally modified in the ER. However,
420 viral glycoproteins can impose an acute burden on the ER when they are rapidly synthesized in
421 large numbers in a relatively brief time frame. This burden may differ in severity depending on

422 the extent of shutoff of host gene expression, as viruses with efficient host shutoff mechanisms
423 would deplete host glycoproteins and facilitate viral utilization of cellular biosynthetic and
424 secretory apparatus. Viral envelope proteins are often more heavily glycosylated than their host
425 counterparts, which can shield them from antibody recognition. Because N-glycosylation is a
426 dynamic process involving glycan trimming and maturation monitored by lectin chaperones like
427 calnexin and calreticulin, viral infection may impose specific burdens on these components of the
428 ER quality control machinery. This may result in delayed trafficking of glycoproteins through the
429 secretory pathway, leading to their degradation. Finally, it should be noted that viral glycoproteins
430 are often assembled into large homo- and hetero-oligomeric complexes that must traffic to sites of
431 assembly. Together, these aspects of viral glycoproteins likely place additional burdens on the ER
432 and associated machinery that governs glycoprotein folding, modification and trafficking.

433 Because cellular GTPases play important roles in viral glycoprotein biogenesis and
434 trafficking, they may be good targets for host-directed antivirals. Viral assembly occurs at distinct
435 sites like the plasma membrane (influenza A viruses) or the ERGIC (coronaviruses). Small
436 molecules that disrupt efficient viral glycoprotein processing, oligomerization and trafficking
437 could have the effect of 'misplacing' these important viral components and inhibiting essential
438 steps in viral assembly and egress. We speculate that 6-TG and 6-TGo inhibit GTPases involved
439 in key steps of viral glycoprotein synthesis, processing and trafficking, diverting them from their
440 roles in viral assembly and consigning them to degradation via cellular catabolic processes. While
441 these drugs are well-tolerated in humans, we believe that more can be gained by identifying and
442 characterizing their mode of action against the GTPases that have thus far been elusive.

443

444 **MATERIALS AND METHODS**

445 **Cell lines.** Human embryonic kidney 293T and 293A cells, human hepatoma Huh-7.5 (66) and
446 African green monkey kidney Vero cells were all maintained in Dulbecco's modified Eagle's
447 medium (DMEM; ThermoFisher Scientific) supplemented with 10% fetal bovine serum (FBS,
448 ThermoFisher Scientific), 100 U/mL penicillin, 100 µg/mL streptomycin, and 2 mM L-
449 glutamine (Pen/Strep/Gln; ThermoFisher Scientific, 15140122 and 25030081). HCT-8 cells were
450 cultured as above with additional 1X MEM Non-Essential Amino Acids (NEAA, Gibco)
451 supplemented. Baby hamster kidney (BHK-21) were maintained as above yet supplemented with

452 5% FBS. African green monkey kidney Vero'76 and human lung adenocarcinoma Calu-3 cells
453 were maintained in DMEM (Sigma-Aldrich, D5796; St. Louis, MO, USA) supplemented with
454 10% fetal bovine serum (ThermoFisher Scientific, 16000-044) and 1X Penicillin-Streptomycin
455 (Gibco, 15140148). hTert-immortalized human foreskin fibroblast (BJ) cells (a kind gift from
456 William Hahn, Dana-Farber Cancer Institute, Boston, USA) cells were maintained in a 4:1 blend
457 of knockout DMEM and medium 199 (ThermoFisher Scientific) with 15% FBS and
458 Pen/Strep/Gln. All cells were maintained at 37°C in 5% CO_2 atmosphere. To generate 293A-
459 ACE2 cells, 293A cells were stably transduced with a lentivirus vector encoding ACE2 (pLJM1-
460 ACE2-BSD) or an empty vector control (pLJM1-B*) (67), then selected and maintained in 10
461 µg/mL Blasticidin S HCl (ThermoFisher, A11139030).
462
463 **Chemical Inhibitors.** 6-thioguanine (6-TG, A4882), 2-amino-6-mercaptopurine riboside hydrate
464 (6-TGo, 858412), 6-mercaptopurine (6-MP, 38171), brefeldin A (BFA; B7651), CASIN
465 (SML1253), ML-099 (SML1258), Rac1 inhibitor V (5308200001), rhosin (555460),
466 thapsigargin (Tg) and tunicamycin (TM) were all purchased from Sigma-Aldrich. N9-methyl 6-
467 thioguanine (6-TGMe) was synthesized in house as described in Supporting Information. All
468 drugs were solubilized in dimethyl sulfoxide (DMSO) and stored at -80˚C. Stock concentrations
469 were diluted to the indicated concentrations in cell culture media.
470
471 **Human coronavirus infections and quantitation.** Stocks of severe acute respiratory syndrome
472 coronavirus 2 (SARS-CoV-2) were propagated in Vero'76 cells (for strain SARS-CoV-
473 2/Canada/ON/VIDO-01/2020, used in Fig. 1A) or Vero E6 cells (SARS-CoV-2/SB3-TYAGNC,
474 used in Figs. 3A, 3B). To generated virus stocks, cells were infected at a low MOI for 1h in
475 serum-free DMEM then incubated at 37°C in DMEM supplemented with 2% FBS and 1X
476 Pen/Strep. Once CPE reached 75% at 2-3 d post-infection, the viral supernatant was harvested,
477 centrifuged at 5000 x *g* for 5 min, and then the cleared viral supernatant was aliquoted and stored
478 at -80°C. Stocks were titered by plaque assay on Vero E6 cells (68) or TCID50 on Vero'76 cells
479 calculated using the Spearman-Kärber method.
480 Stocks of human coronavirus OC43 (hCoV-OC43; ATCC, VR-1558) were propagated in
481 Vero cells. Cells were infected at a MOI of 0.05 for 1 h at 33°C in serum-free DMEM. After 1 h,
482 the infected cells were maintained in DMEM supplemented with 1% FBS and Pen/Strep/Gln for

483 five days at 33°C. Upon harvest, the culture supernatant was centrifuged at 1000 x *g* for 5 min at
484 4°C, aliquoted, and stored at -80°C. Stocks of human coronavirus 229E (hCoV-229E; ATCC,
485 VR-740) were prepared similarly to hCoV-OC43 yet using Huh-7.5 cells and DMEM
486 supplemented with 2.5% FBS and Pen/Strep/Gln. Viral titers were enumerated by median tissue
487 culture infectious dose ($TCID_{50}$) assays. Following the serial dilution of the samples, the
488 appropriate cell line was infected for 1 h at 37°C prior to the replacement of the inoculum for the
489 indicated overlay medium and incubated at 37°C: BHK-21 cells (hCoV-OC43,
490 DMEM/1%FBS/Pen/Strep/Gln, 5 days), Huh-7.5 cells (hCoV-229E,
491 DMEM/2.5%FBS/Pen/Strep/Gln, 4 days), or Vero'76 cells (SARS-CoV-2,
492 DMEM/2%FBS/Pen/Strep/Gln, 5 days). Viral titers were calculated using the Spearman-Kärber
493 method.
494 To test the effect of the indicated compounds on hCoV replication, 293A, 293T, BJ,
495 Calu-3, HCT-8, or Huh-7.5 cells were infected with hCoV diluted in serum-free DMEM at the
496 indicated MOI and temperature for 1 h. After 1 h, the inoculum was removed, replaced with
497 DMEM/Pen/Strep/Gln containing 1% FBS and NEAA (HCT-8), 2% FBS (Calu-3), 2.5% FBS
498 (Huh-7.5, 293A or 293T), or 5% FBS (BJ) supplemented with DMSO or drug at the indicated
499 concentration, and maintained for an additional 23 h at the indicated temperature. Infected BJ
500 cells were incubated at 33°C during virus replication; all other cells were incubated at 37°C. For
501 infections of 293A, BJ, HCT-8, or Huh-7.5, the infected cells were scraped into the culture
502 medium and stored at -80°C. For SARS-CoV-2-infected Calu-3 cells or HCoV-OC43 infected
503 293T cells virus was collected from culture supernatants at 48 h post-infection and stored at -
504 80°C. Titers of hCoV-OC43, hCoV-229E, and SARS-CoV-2 were determined using $TCID_{50}$
505 assays as indicated above.
506
507 **Cytotoxicity assays.** Cells seeded into 96-well tissue culture plates were treated with drugs
508 diluted at indicated concentrations and incubated with the cells for 20 h. At 20 h post-treatment,
509 10% alamarBlue Cell Viability Reagent (ThermoFisher Scientific, DAL1025) diluted in
510 DMEM/Pen/Strep/Gln containing 1% FBS and NEAA (HCT-8), 2.5% FBS (Huh-7.5 or 293T),
511 or 5% FBS (BJ) was added and further incubated for 4 h. Plates were read on FLUOstar Omega
512 96 well plate reader at an excitation of 544 nm, and an emission of 580-590 nm. Drug treatments
513 were then normalized to DMSO. For viability experiments using Calu-3 cells, cells grown in 96-

514 well plates were treated with drugs diluted at indicated concentrations and incubated with the
515 cells for 48 h. At 48 h post-treatment, a one-fifth volume of CellTiter 96 AQueous One Solution
516 Cell Proliferation Assay (G3580, Promega) was added to DMEM/Pen/Strep containing 2% FBS
517 and incubated for 2 h. Plates were read at an absorbance of 490 nm with an xMark™ Microplate
518 Absorbance Spectrophotometer (Bio-Rad). Values were imported into GraphPad PRISM (v.9)
519 and CC_{50} values were calculated by fitting a non-linear curve to the data. Selectivity index (SI)
520 was calculated by dividing the IC_{50} (calculated above) by the CC_{50}.
521
522 **Real-time quantitative PCR.** Total RNA from cells was extracted using the RNeasy Plus Mini
523 Kit (QIAGEN, 74134) following the manufacturer's protocol. Synthesis of cDNA was
524 performed using the Maxima H Minus First Strand cDNA Synthesis Kit (ThermoFisher
525 Scientific, K1652) using random primers. Quantitative PCRs were performed using 200 nM
526 primers, 1:250 (final) diluted cDNA, and 1X GoTaq qPCR Master Mix (Promega, A6002).
527 Amplifications were performed using a CFX Connect Real-Time PCR Detection System (Bio-
528 Rad) and Bio-Rad CFX Manager 3.1 software. To measure supernatant virions, supernatant was
529 mixed 1:1 with virus lysis buffer [20 mM Tris HCl pH7.4, 300 mM NaCl, 2.5% NP-40, and 40
530 U/mL RNAaseOUT (ThermoFisher)] for 5 min, then diluted 1:5 with nuclease-free water before
531 2 µL was used as template in a 10 µL Go-Taq 1-Step RT-qPCR (Promega, A6020) reaction (69).
532 Primer sequences are listed in Table 1.
533
534 **Immunofluorescence microscopy.** 293T were seeded on #1.5 coverslips (Zeiss, 411025-0003-
535 000) coated with poly-L-lysine (Sigma, P2658). The following day the cells were infected with
536 HCoV-OC43, to harvest the cells were washed once with 1x Dulbecco's PBS (ThermoFisher)
537 and fixed with 4% paraformaldehyde (Electron Microscopy Services) PBS for 15 min at room
538 temperature. Coverslips were blocked and permeablized in staining buffer [1% human serum
539 (Sigma,4552) heat-inactivated at 56°C for 1h, 0.1% Triton X-100 PBS] for 1 h at room
540 temperature, then stained with 1:500 dilution anti-OC43 N (MAB9012, Millipore Sigma)
541 overnight at 4°C. The following day the coverslips were washed three times with PBS, then
542 stained with goat anti-mouse Alexa 488 (ThermoFisher, R37120) in staining buffer for 1 h at
543 room temperature in the dark. Coverslips were then counterstain for 5 min with Hoescht 33342
544 (ThermoFisher, 62249), washed three times with PBS, then mounted on coverglass using

545 ProLong Gold anti-fade reagent (ThermoFisher, P36930). Z-stacks were imaged on a Zeiss
546 LSM880 and processed into maximum intensity projections using Zen Black (Zeiss).
547
548 **Western Blotting.** Cell monolayers were washed once with ice-cold PBS and lysed in 2x
549 Laemmli buffer (4% [wt/vol] sodium dodecyl sulfate (SDS), 20% [vol/vol] glycerol, 120 mM
550 Tris-HCl [pH 6.8]). DNA was sheared by repeated pipetting with a 21-gauge needle before
551 adding 100 mM dithiothreitol (DTT) and boiling at 95˚C for 5 min. Samples were stored at -20˚C
552 until analysis. Total protein concentration was determined by DC protein assay (Bio-Rad) and
553 equal quantities were loaded in each SDS-PAGE gel. For ribopuromycylation assays, a modified
554 version of the protocol by Schmidt, *et al.* (63) was used where the indicated samples were treated
555 with 10 µg/ml puromycin (ThermoFisher, A1113803) for 10 min, followed by a PBS wash, and
556 lysate preparation for immunoblotting as indicated above. Lysates from the ribopuromycylation
557 assays were loaded into gels prepared using the TGX Stain-Free FastCast Acrylamide Kit (Bio-
558 Rad, 1610183) (Fig. S1A). Lysates for quantitative Spike western blotting were loaded onto
559 TGX Stain-Free 4-20% gradient gels (Bio-Rad, 4568094) (Fig. 3D). Peptide-*N*-Glycosidase F
560 (PNGase F; NEB, P0704) treatment of lysates was performed as described in the manufacturer's
561 directions. All proteins after SDS-PAGE were transferred to polyvinylidene difluoride (PVDF)
562 membranes (Bio-Rad) with the Trans-Blot Turbo transfer apparatus (Bio-Rad). Membranes were
563 blocked with 5% bovine serum albumin in tris-buffered saline/0.1% [vol/vol] tween-20 (TBS-T)
564 before probing overnight at 4˚C with antibodies raised to the following targets: mouse anti-
565 puromycin (Millipore-Sigma, MABE343), mouse anti-OC43 N (CoV antibody, OC43 strain,
566 clone 541-8F, Millipore-Sigma, MAB9012), rabbit anti-BiP (Cell signaling Technologies (CST),
567 mouse anti-XBP1s (CST, #12782), mouse anti-CHOP (CST, #2895), rabbit anti-α-Tubulin (CST,
568 #2125), rabbit anti-SARS-CoV-2 S1 RBD (Elabscience, E-AB-V1006), anti-SARS-CoV-2 E
569 (abbexa, abx226552), anti-SARS-CoV-2 M (Novus Biologicals, NBP3-05698), rabbit anti-
570 SARS-CoV-2 N (Novus Biologicals, NBP3-05730), mouse anti-FLAG (CST, #2368), mouse
571 anti-HIV-p24 (Abcam, ab9071) anti-Strep tag (IBA, 2-1507-001), anti-HRPT1 (Santa Cruz
572 Biotechnologies, sc-376938)and anti-β-actin (CST, #4967). Membranes were washed with TBS-
573 T and incubated with HRP-linked secondary antibodies prior to detection with Clarity ECL
574 chemiluminescence reagent (Bio-Rad). All blots were imaged on a Bio-Rad ChemiDoc-Touch
575 system. Molecular weights were determined using the Broad Range, Color Prestained Protein

576 Standard (NEB, P7719) or Precision Plus Protein All Blue Prestained Protein Standards (BioRad,
577 1610373). Molecular weights in kDa are indicated on the left of blot images. For quantitation of
578 western blots, the total antibody signal intensity was divided by the Stain-Free total protein
579 signal. Images were analyzed using Image Lab 6.1 (Bio-Rad). Images were cropped and
580 annotated using Affinity Designer (Serif).
581
582 **Plasmid generation and transfections.** All plasmids were purified using the QIAprep Spin
583 Miniprep or QIAfilter Plasmid Midi Kits (QIAGEN) and all restriction enzymes were purchased
584 from New England Biolabs (NEB). The pcDNA3-SARS-CoV-2-Spike plasmid contains a
585 codon-optimized ORF for Spike from GenBank NC_045512 that was synthesized by GenScript
586 (a kind gift from David Kelvin) then cloned between the KpnI and BamHI sites of pcDNA3.1(+).
587 A 19 residue C-terminal truncation of Spike (SΔ19) and Spike with a C-terminal FLAG tag was
588 generated by PCR. A Spike mutant lacking the Furin cleavage site between S1 and S2 (P681S,
589 R682G, R683G, R685del), and two-proline stabilizing mutants, K986P and V987P (S-2P) (70–
590 72) was generated by PCR mutagenesis using KOD Xtreme Hot Start DNA Polymerase (Sigma,
591 71975-M). pcDNA3-Membrane (M) and pcDNA3-Envelope (E) were cloned from pLVX-
592 EF1alpha-SARS-CoV-2-M-2xStrep-IRES-Puro and pLVX-EF1alpha-SARS-CoV-2-E-2xStrep-
593 IRES-Puro (kind gifts from Neven Krogan, available from Addgene #141386 and #141385)
594 using PCR to remove the 2xStrep epitope tag. pCMV3-MERS-FLAG was purchased from
595 SinoBiologicals (VG40069-CF). pLJM1-Luc2 used in generating Spike-pseudotyped
596 lentiviruses was generated by cloning Luc2 from pGL4.26 (Promega) into pLJM1-B* (67).
597 pLJM1-ACE2-BSD was cloned by from cDNA of generated from Caco-2 cells. Primer
598 sequences are listed in Table 2. 293T cells were transfected using polyethylenimine (PEI),
599 Linear, MW 25000 (Polysciences Inc., 23966) dissolved in water (pH 7.4). Both plasmids and
600 PEI were diluted in OptiMEM (Gibco), then combined for 15 min before adding to cell
601 monolayers in serum-free DMEM. PEI was used at 3:1 ratio to plasmid DNA. After 4 h, serum-
602 free media was replaced with DMEM containing 10% FBS with indicated treatments unless
603 otherwise indicated. For pre-treatments with ML099. the drug was applied at the time of
604 transfection, then refreshed when the media was changed 4 h after transfection. Generally, cells
605 were lysed for immunoblotting analysis at 24 h post-transfection (hpt). For flow-cytometry and

606 immunofluorescence experiments, cells were instead transfected with FugeneHD (Promega,
607 E2311) according to the manufacturer's instructions.
608

609 **siRNA knockdown experiments.** All siRNAs were obtained from Invitrogen. 293T cells (1-1.5
610 x 10^5 cells/mL) in 10% DMEM were reverse transfected with Lipofectamine RNAiMAX
611 (Invitrogen, 13778075) and 10 nM of Silencer Select negative siRNA #2 (4390846), HPRT1
612 siRNA #1 (s6889), or HPRT1 siRNA #2 (s6888) diluted in OptiMEM (Gibco, 31985070). RNA
613 was harvested from cells 48 hpt knockdown validation by RT-qPCR. For determining the effect
614 of HPRT1 knockdown on viral titre after 6-TG treatment, the reverse transfected cells were
615 infected at 24 hpt at an MOI of 0.1 then treated with DMSO or 10 µM 6-TG as described above.
616 After a 24 h infection, the cell supernatant for titration, and the infected monoloayers were lysed
617 with 2X Laemmli Buffer and processed for western blotting.

618

619 **Production of SARS-CoV-2 virus-like particles.** To generate SARS-CoV-2 virus-like
620 particles, 293T cells were seeded in a 10 cm dish and co-transfected with 2 µg of each pcDNA-
621 Spike, pcDNA-M, pcDNA-E, and pLVX-EF1alpha-SARS-CoV-2-N-2xStrep-IRES-Puro (a kind
622 gift from Neven Krogan, available from Addgene #141391) with PEI, then treated with 6-TG or
623 DMSO as described above. After two days, supernatant was harvested, filtered, concentrated,
624 and analyzed by western blot as described above for SARS-CoV-2 Spike-pseudotyped lentivirus.

625

626 **SARS-CoV-2 Spike-pseudotyped lentiviruses.** To generate Spike-pseudotyped lentivirus
627 particles, 293T cells were seeded in a 10 cm dish and co-transfected with 3 µg pLJM1-Luc2, 2
628 µg pSPAX2 (a kind gift from Didier Trono; Addgene #12260), and 2 µg of pcDNA3- SΔ19 with
629 PEI, then treated with 6-TG or DMSO as described above. After two days, supernatant was
630 harvested, filtered through a 0.45 µm filter, aliquoted and stored at -80°C until use. Genomes
631 were quantified using a qPCR Lentivirus Titer Kit (Applied Biological Materials, LC900) as per
632 the manufacturer's instructions. Infectious pseudotyped particles were measured by infecting
633 293A cells stably expressing ACE2 or an EV control. Cell lysates were harvested 24 h after
634 infection in Reporter Lysis Buffer (Promega, E397A), lysed by freeze thawing at -80°C, and
635 luciferase activity was measured using Luciferase Assay reagent (Promega) on a FLUOstar

636 Omega microplate reader (BMG Labtech). For concentration and western blot analysis, filter
637 supernatant was underlaid with 20% sucrose PBS using a pipetting needle and centrifuged at 39
638 000 rpm for 2 h using an SW-41 rotor (Beckman Coulter). The supernatant and sucrose solution
639 were carefully removed, and the pellet was resuspended in PBS, mixed in equal proportions with
640 2x Laemmli Buffer with 100 mM DTT and boiled at 95°C for 5 min before analysis by western
641 blot.

642

643 **Transmission electron microscopy (TEM).** Samples were prepared and visualized as described
644 in (73). Briefly, HCoV-OC43 containing supernatant was concentrated by ultracentrifugation as
645 described above, then applied to Formvar/carbon coated grids and left to settle to 10 min. The
646 grid was then rinsed with distilled water then stain with 2% w/v uranyl acetate for 30 s. Residual
647 stain was wicked off with filter paper then left to air dry completely. Grids were imaged on a
648 JEM 1230 TEM (JEOL) running at 80 kV using an OCRA-HR camera (Hamamatsu). Sample
649 preparation, fixation, and TEM imaging were performed twice with representative images from
650 one independent experiment shown.

651

652 **Quantitation of SARS-CoV-2 Spike surface expression.** 293T cells were co-transfected with
653 pEGFP-N1 and plasmids expressing SARS-CoV-2 Spike (FL) or SARS-CoV-2 Spike-Δ19 for
654 24 h using FugeneHD (Promega). The cells were treated with DMSO or 10 µM 6-TG at 4 h post-
655 transfection. At 24 h post-transfection, the cells were lift with 10 mM EDTA PBS and pelleted at
656 300 x *g* for 5 min. Cells were washed once with wash buffer (2 mM EDTA, 2% FBS, PBS), then
657 stained with 0.1 µg/sample Alexa Fluor 647-conjugated mouse-anti SARS-CoV-2 Spike S1
658 (R&D Systems, FAB105403R-100UG) at 4°C for 30 min in the dark. Cells were then washed
659 then fixed with 2% paraformaldehyde (Electron Microscopy Sciences, 15710) PBS 4°C for 30
660 min in the dark, then washed and stored at 4°C in the dark until analysis using a FACSCelesta
661 cell analyzer (BD Biosciences) configured with 405 nm, 488 nm, and 640 nm lasers using the
662 same acquisition voltages for all replicates with at least 50000 single cells acquired per sample.
663 The data were analyzed using FCS Express v. 6.06.0040 (De Novo Software) where transfected
664 single cells were selected by EGFP fluorescence and analyzed for Spike surface expression via
665 Alexa Fluor 647 fluorescence.

666

667 ***Gaussia* luciferase secretion assays.** For short-term treatments, 293T were transfected with
668 pCMV-*Gaussia* Luc Vector (ThermoFisher Scientific, 16147) as described above. After 18 h,
669 medium was removed and replaced with fresh medium containing 6-TG, BFA, or DMSO. After
670 6 h medium was removed, debris was cleared by centrifuging samples at 5,000 × *g* for 5 min,
671 then samples were stored at -80°C until measuring *Gaussia* luciferase activity using the *Gaussia*
672 Luciferase Flash Assay Kit (ThermoFisher Scientific, 16158) as per the manufacturer's
673 directions on a FLUOstar Omega microplate reader (BMG Labtech). For long-term treatments,
674 293T cells were co-transfected with pCMV-*Gaussia* Luc and pLJM1-Luc2 and treated 6 h post
675 transfection. After 24 h, supernatant harvested as described above. The cell monolayer was lysed
676 in Reporter Lysis Buffer (Promega) as described above. To measure both Luciferase and *Gaussia*
677 luciferase activity in samples, we used the Dual-Luciferase Reporter Assay System (Promega,
678 E1910), which although designed for firefly and *Renilla* luciferase, can be readily adapted for
679 firefly and *Gaussia* luciferase as both *Gaussia* and *Renilla* luciferase both use coelenterazine as a
680 substrate.

681

682 **Statistical analysis.** Statistical analysis and graphing was performed using GraphPad PRISM
683 (v.8 or v.9). Statistically significant differences were determined using Dunnett's multiple
684 comparison test for one-way ANOVA and Šídák's multiple comparison test for two-way
685 ANOVA.

686

687 **Graphics.** Molecular models were created with NCBI PubChem
688 (http://pubchem.ncbi.nlm.nih.gov/) The model presented in Fig. 7 was adapted from
689 "Coronavirus Replication Cycle", by BioRender.com (2022). Retrieved from
690 https://app.biorender.com/biorender-templates.

691

692 **ACKNOWLEDGEMENTS**

693 We are grateful for the support of the Dalhousie University Flow Cytometry Core Facility and
694 the Cellular and Molecular Digital Imaging Core Facility. This work was supported by Canadian

695 Institutes for Health Research (CIHR) Project Grant PJT-148727 (to C.M.), Natural Sciences and
696 Engineering Research Council (NSERC) of Canada Discovery Grant RGPIN-2016-05083 (to
697 S.L.B.), Coronavirus Variants Rapid Response Network (CoVaRR-Net) Grant 175622 (to J.A.C.
698 and others), Research Nova Scotia Grant RNS-NHIG-2020-1383 and Lung Association of Nova
699 Scotia Legacy Research Grant (to D.K.), and a Nova Scotia COVID-19 Health Research
700 Coalition Grant to C.M. and E.S.P. SARS-CoV-2 research is supported in the laboratory of D.F.
701 by the Canadian Institutes of Health Research (CIHR; OV5-170349, VRI-173022 and VS1-
702 175531). VIDO receives operational funding from the Government of Saskatchewan through
703 Innovation Saskatchewan and the Ministry of Agriculture and from the Canada Foundation for
704 Innovation through the Major Science Initiatives for its CL3 facility.
705

706 **CONFLICT OF INTEREST**

707 E.S.P. is a consultant for Aegis Life Inc. All other authors declare no conflicts of interest.
708

709 **FIGURE LEGENDS**

710

711 **Table 1**. Primer sequences for RT-qPCR analysis

Target	Sequence (5′-3′)	
OC43 Orf1a	F – ATATGGCCAAGGCTGGTGAC	R – ATGTAACACGCCTTCCAGCA
OC43 S	F – TCTTCCGAACCAGCATTGCT	R – TAATGGGTTGCAGCTGTCGT
OC43 N	F – GGACCCAAGTAGCGATGAGG	R – GTGCGCGAAGTAGATCTGGA
18S	F – TTCGAACGTCTGCCCTATCAA	R – GATGTGGTAGCCGTTTCTCAGG
HPRT1	F – CGAGATGTGATGAAGGAGATG	R – GCAGGTCAGCAAAGAATTTATAG
Xbp1	F – TAGCAGCTCAGACTGCCAGA	R – CCAAGCGCTGTCTTAACTCC
ERdj4	F – CGCCAAATCAAGAAGGCCT	R – CAGCATCCGGGCTCTTATTTT
EDEM1	F – TTGACAAAGATTCCACCGTCC	R – TGTGAGCAGAAAGGAGGCTT
ATF3	F – AGGCGACGAGAAAGAAATAAG	R – TTCACACTTTCCAGCTTCTC
CHOP	F – ATGAACGGCTCAAGCAGGAA	R – GGGAAAGGTGGGTAGTGTGG
HERPUD1	F – AACGGCATGTTTTGCATCTG	R – GGGGAAGAAAGGTTCCGAAG

BiP	F – GCCTGTATTTCTAGACCTGCC	R – TTCATCTTGCCAGCCAGTTG

712

713

714

715 **Table 2.** Primers used for cloning and PCR mutagenesis

Gene	Sequence (5′-3′)
Spike	F - AATTGGTACCATGTTCGTCTTTCTGGTTCTGTTGCC
	R - AATTGGATCCTCAAGTGTAGTGCAGTTTCACGC
Spike-S0	F - CTCCGTGGCAAGCCAGTCGATCATCGCCTAC
	R - GCGCCTCCACTCGAGTTCGTCTGGGTCTGGTA
Spike-Flag	F - AATTGGTACCATGTTCGTCTTTCTGGTTCTGTTGCC
	R - AATTGGATCCTTACTTATCGTCGTCATCCTTGTAAT CAGAGCCTCCACCCCCAGTGTAGTGCAGTTTCACGC
Spike-Δ19	F - AATTGGTACCATGTTCGTCTTTCTGGTTCTGTTGCC
	R - AATTGGATCCTTAACAACAACTACCGCAACTGC
Spike-2P	F - CCGGAGGCCGAGGTGCAGATCGAC
	R - TGGGTCCAGTCTTGACAGGATGTCGTTC
E	F - AATTGCTAGCACCATGTACAGCTTCG
	R - AATTGAATTCTTAAACGAGGAGATCCGGCAC
M	F - AATTGCTAGCACCATGGCCGACTCAAATGG
	R - AATTGAATTCTTACTGGACGAGTAAAGC
ACE2	F - AATTACCGGTATGTCAAGCTCTTCCTGGC
	R - AATTGTCGACCTAAAAGGAGGTCTGAACATCATCAG

716

717

718

719 **Figure 1. Thiopurines 6-thioguanine and 6-thioguanosine inhibit coronavirus replication.**
720 **(A)** Structures of thiopurines used this study in comparison to Guanosine. **(B)** Calu-3 cells were
721 infected with SARS-CoV-2 at an MOI of 0.1 then treated with 6-thioguanine (6-TG), 6-
722 thioguanosine (6-TGo), or 6-mercaptopurine (6-MP). Supernatant was harvested after 48 h and
723 stored at -80ºC until titering on Vero'76 cells. Mock-infected cells were similarly treated with 6-
724 TG, 6-TGo, 6-MP, or DMSO vehicle control for 48 h before testing cell viability with CellTiter
725 98 AQueous One (n=3 ± SEM). **(C)** Summary table of Cellular Cytotoxicity (CC_{50}), Effective
726 concentration (EC_{50}), and Selectivity Index (SI) calculated for (A-C). **(D)** Alamar Blue cell
727 viability assay of hTert-BJ, HCT-8, and Huh-7.5 cells treated with 6-TG (n=3±SEM).**(E)** TCID
728 assays for HCoV-OC43 infected HCT-8 cells and **(F)** HCoV-229E infected Huh-7.5. Cells were
729 infected with an MOI of 0.1 then treated with 6-TG, 6-TGo, 6-MP, or DMSO (n=3 ± SEM,
730 statistical significance was determined by one-way ANOVA). **(F)** hTERT-BJ cells were infected
731 with HCoV-OC43 or HCoV-229E at an MOI of 0.1 and treated with 6-TG, Tm, or DMSO.
732 Supernatant was harvested after 23 h and stored at -80∞C before titering on BHK-21 or Huh7.5
733 (n=3-4 ± SEM, statistical significance was determined by one-way ANOVA). **(G)** hTERT-BJ
734 cells were infected with HCoV-OC43 or **(H)** HCoV-229E at an MOI of 0.1 and treated with 6-
735 TG, Tm, or DMSO. Supernatant was harvested after 23 h and stored at -80∞C before titering on
736 BHK-21 or Huh7.5 (n=3-4 ± SEM, statistical significance was determined by one-way
737 ANOVA). LoD = Limit of Detection for virus titer. (*, $p<0.05$; **, $p<0.01$; ns, non-significant)
738
739 **Figure 2. 6-TG reduces CoV protein and mRNA accumulation. (A-C)** 293T cells were
740 infected with HCoV-OC43 at an MOI of 0.1 then treated with 10 μM 6-TG or DMSO vehicle
741 control. Supernatant and total RNA from the cells were harvested at the times indicated and

742 stored at -80ºC until **(A)** titering on BHK-21 or **(B)** quantification of viral genomes by RT-qPCR.
743 Cell monolayers were harvested for **(C)** RT-qPCR analysis of viral RNA accumulation (n=3
744 statistical significance was determined by paired ratio t test; *, $p<0.05$; **, $p<0.01$; ns, non-
745 significant) **(D)** 293T cells were grown on coverslips then infected with HCoV-OC43 and treated
746 with 6-TG as in (A), then fixed and immunostained for N or **(E)** dsRNA. Nuclei are
747 counterstained with Hoechst. Scale bar = 20 µm.
748
749 **Figure 3. 6-TG inhibits Spike glycosylation and cleavage. (A)** Calu-3 cells were with SARS-
750 CoV-2 at an MOI of 7, then treated with 6-TG or DMSO. Lysates were harvested 48 h after
751 transfection and were probed by western blotting as indicated. Concentrations in legend are in
752 µM. **(B)** Huh-7.5 cells were with SARS-CoV-2 at an MOI of 5, then treated with 6-TG or
753 DMSO. Lysates were harvested 48 h after transfection and were probed by western blotting as
754 indicated. Concentrations in legend are in µM. **(C)** 293T cells were transfected with SARS-CoV-
755 2 S, M, Envelope (E), Nucleoprotein (N) with a C-terminal 2xStrep tag, or EV then treated with
756 10 µM 6-TG or DMSO vehicle control. Lysates were harvested 24 h after transfection and
757 probed by western blotting as indicated. **(D)** 293T cells were transfected with SARS-CoV-2
758 Spike or EV then treated with 6-TG or DMSO vehicle control. Lysates were harvested 24 h after
759 transfection and were probed by western blotting as indicated. Concentrations in legend are in
760 µM. **(E)** Alamar Blue cell viability assay of 6-TG treated 293T cells (n=3±SEM). **(F)** 293T cells
761 were transfected with SARS-CoV-2 Spike (S), a Spike mutant lacking the Furin cleavage site
762 between S1 and S2 (S0), or EV then treated with 10 µM 6-TG or DMSO vehicle control. Lysates
763 were harvested 24 h after transfection, treated with PNGase F to remove N-linked glycans, and

764 probed by western blotting as indicated. **(G)** as in (C) except 293T cells were transfected with C-
765 terminal FLAG-tagged Spike (S-FL) or HCoV-MERS Spike (MERS).
766
767 **Figure 4. 6-TG stimulates an assembly defect and inhibits Spike virion incorporation. (A)**
768 293T cells were transfected with equal quantities of SARS-CoV-2 S, M, E, and N or empty
769 vector (EV) then treated with 10 µM 6-TG or DMSO vehicle control. Lysates were harvested 48
770 h after transfection and probed by western blotting as vindicated. **(B)** Virus-like particles from
771 supernatants of cells transfected in (B) were concentrated by ultracentrifugation through a 20%
772 sucrose cushion, resuspended in PBS, then harvested with an equal volume of 2x Leammli
773 buffer. Samples from two independent lentivirus preparations were probed by western blotting as
774 indicated. **(C)** 293T cells were transfected with S, E, M, and N in a 1:2:2:1 ratio, substituting one
775 of the structural proteins for EV as indicated, treated with 6-TG or DMSO then processed as in
776 (A). **(D)** SARS-CoV-2 Spike pseudotyped, luciferase-expressing lentivirus particles were
777 concentrated by ultracentrifugation through a 20% sucrose cushion, resuspended in PBS, then
778 harvested with an equal volume of 2x Leammli buffer. Samples from three independent
779 lentivirus preparations were probed by western blotting as indicated. **(E)** Genomes from three
780 independent lentivirus preparations were quantified by RT-qPCR (n=3, statistical significance
781 was determined by paired t-test; ns, non-significant). **(F)** 293A cells stably expressing ACE2 or
782 an empty vector control were transduced with lentivirus from three independent preparations.
783 After 24 h, lysates were harvested and measured for luciferase activity (n=3, statistical
784 significance was determined by two-way ANOVA; *, $p<0.05$; ns, non-significant). **(G)** 293A
785 cells were infected HCoV-OC43 at an MOI of 0.1 =, then treated with 6-TG or DMSO.
786 Supernatants were concentrated as in (C), before virions were fixed and imaged and imaged by

787 TEM with negative staining. Five virions from both 6-TG- and DMSO-treated samples are
788 shown at 150,000 X magnification. Scale bar = 100 nm.
789
790 **Figure 5. 6-TG inhibits Spike maturation through GTPase inhibition. (A)** 6-TG is
791 conjugated to phosphoribosyl diphosphate (PRPP) by HPRT1 to form 6-TG monophosphate. 6-
792 TG methylated at the N9 nitrogen was designed to be resistant to processing by HPRT1. **(B)**
793 293T cells were infected with HCoV-OC43 at an MOI of 0.1 then treated with 6-TG or 6-TG-
794 Me. Supernatant was harvested at the times indicated and stored at -80∞C until titering on BHK
795 cells. (n=3 statistical significance was determined by paired ratio t test; *, $p<0.05$; **, $p<0.01$; ns,
796 non-significant). **(C)** 293T cells were transfected with SARS-CoV-2 Spike or an empty vector
797 control then treated with 6-TG, 6-TG-Me, or DMSO vehicle control. Lysates were harvested 24
798 h after transfection, treated with PNGase F to remove N-linked glycans, and probed by western
799 blotting as indicated. **(D)** 293T cells were reversed transfected with siRNA and total RNA was
800 harvested after 48 h. HPRT1mRNA abundance was measured by RT-qPCR (n=3, ±SEM
801 statistical significance was determined by one way ANOVA; ***, $p<0.001$). **(E)** As in D but
802 cells were infected with HCoV-OC43 at an MOI of 0.1 24 h after siRNA treatment and
803 supernatant was harvested and titered as in **(B)** (n=4 ±SEM statistical significance was
804 determined by paired ratio t test; **, $p<0.01$; ***, $p<0.001$; ns, non-significant).
805
806 **Figure 6. 6-TG inhibits Spike maturation through GTPase inhibition. (A)** Alamar Blue cell
807 viability assay of 293T cells treated Rac1 Inhibitor V (Rac1iV), Rhosin, CASIN, or ML099
808 (n=3±SEM). **(B)** Summary table of Cellular Cytotoxicity (CC_{50}) and inhibitor target of
809 compounds tested in (A). **(C)** 293T cells were transfected with SARS-CoV-2 Spike or an empty

810 vector control (EV) then treated with 6-TG, GTPase inhibitors, or DMSO vehicle control.
811 Concentrations in legend are in µM. Lysates were harvested 24 h after transfection and were
812 probed by western blotting as indicated. **(D)** 293T cells were transfected with plasmids encoding
813 Spike or EV then co-treated with 6-TG, 100 µM ML099 GTPase agonist, or DMSO. Lysates
814 were harvested 24 h after transfection and were probed by western blotting as indicated.
815 Concentrations in legend are in µM **(E)** as in (D) except some samples were pre-treated (Pre) for
816 4 h with ML099. **(F)** HCT-8 and 293A were infected with an MOI of ~0.1 then treated with 10
817 µM 6-TG or DMSO vehicle control. After 24 h, the supernatants were harvested and stored at -
818 80∞C until titering on BHK-21 (n=3 ± SEM, statistical significance was determined by one-way
819 ANOVA; *, p<0.05; **, p<0.01; ns, non-significant). LoD = Limit of Detection for virus titer.
820
821 **Figure S1. Activation of the unfolded protein response (UPR) during OC43 infection. (A)**
822 293T cells were infected with HCoV-OC43 at an MOI of 0.1 then treated with 10 µM 6-TG or
823 DMSO vehicle control. Total RNA from the cells were harvested at the times indicated and
824 stored at -80∞C until RT-qPCR analysis of UPR target genes. **(B)** 293A cells were infected as in
825 (A), then treated with 10 µg 6-TG, 1µg thapsigargin (Tg), or DMSO. Cells were treated with 10
826 µg/mL of puromycin for 10 min prior to harvest 24 h after transfection. Lysates were probed by
827 western blot as indicated. **(C)** Total puromycin intensity from (E) was quantified relative to total
828 protein load and are graphed normalized to the mock-infected, DMSO-treated cells (n=3 ± SEM,
829 statistical significance was determined by paired t-test compared to mock-infected, DMSO-
830 treated cells; *, p<0.05; **, p<0.01; ***, p<0.001; ns, non-significant).
831

832 **Figure S2. 6-TG reduces surface expression of Spike but does not globally limit secretion.**
833 **(A)** Alamar Blue cell viability assay of 293T cells treated with Bafilomycin A (BFA)
834 (n=4±SEM). **(B)** 293T cells were transfected with *Gaussia* luciferase for 18 h then treated with
835 6-TG, BFA or DMSO vehicle control for 6 h. Supernatants were recovered from the cells and
836 measured for luciferase activity. **(C)** 293T cells were transfected with both luciferase and
837 *Gaussia* luciferase then treated with 6-TG, BFA, or DMSO. After 24 h, supernatants were
838 removed and analyzed as in (B). Cell lysate was harvested in Reporter Lysis Buffer and stored at
839 -80∞C until both luciferase and *Gaussia* luciferase activity was measured. (For B and C, n=3 ±
840 SEM, statistical significance was determined by paired t-test compared to DMSO-treated cells; *,
841 p<0.05; **, p<0.01; ***, p<0.001; ns, non-significant). **(D)** 293T cells were transfected with
842 SARS-CoV-2 Spike or EV then treated with 6-TG, BFA, or DMSO. Lysates were harvested 24 h
843 after transfection in 2x Leammli buffer and were probed by western blotting as indicated. **(E)**
844 293T cells were co-transfected with EGFP and either Spike (S), Spike with 19 residue C-
845 terminal truncation (SΔ19), or EV and then treated with 10 μM 6-TG or DMSO. After 24 h, cells
846 were harvested, surface-stained for Spike then fixed prior to analysis by flow cytometry. EGFP+
847 cells were gated for analysis of number of Spike+ cells and Median Fluorescent Intensity (MFI)
848 (n=4±SEM statistical significance was determined by paired t-test between 6-TG and DMSO
849 treated cells; *, p<0.05).
850
851 **Figure 7. 6-TG inhibits multiple essential steps in virus replication and assembly.** 6-TG
852 inhibits nsp3, delaying formation of replication compartments and reducing accumulation of
853 viral RNA. 6-TG also inhibits normal glycosylation of Spike, which fails to be properly

854 packaged in egressing virions. As a result, the total number of virions released from infected

855 cells is reduced and those that are released have fewer Spikes on their surface.

856

857
858
859 **REFERENCES**

860 1. Angelini MM, Akhlaghpour M, Neuman BW, Buchmeier MJ. 2013. Severe acute
861 respiratory syndrome coronavirus nonstructural proteins 3, 4, and 6 induce double-
862 membrane vesicles. mBio 4:e00524-13.

863 2. Gosert R, Kanjanahaluethai A, Egger D, Bienz K, Baker SC. 2002. RNA replication of
864 mouse hepatitis virus takes place at double-membrane vesicles. J Virol 76:3697–3708.

865 3. Knoops K, Kikkert M, Worm SHE van den, Zevenhoven-Dobbe JC, van der Meer Y,
866 Koster AJ, Mommaas AM, Snijder EJ. 2008. SARS-coronavirus replication is supported by
867 a reticulovesicular network of modified endoplasmic reticulum. PLoS Biol 6:e226.

868 4. Beachboard DC, Anderson-Daniels JM, Denison MR. 2015. Mutations across murine
869 hepatitis virus nsp4 alter virus fitness and membrane modifications. J Virol 89:2080–2089.

870 5. Oudshoorn D, Rijs K, Limpens RWAL, Groen K, Koster AJ, Snijder EJ, Kikkert M,
871 Bárcena M. 2017. Expression and Cleavage of Middle East Respiratory Syndrome
872 Coronavirus nsp3-4 Polyprotein Induce the Formation of Double-Membrane Vesicles That
873 Mimic Those Associated with Coronaviral RNA Replication. mBio 8:e01658-17.

874 6. Doyle N, Hawes PC, Simpson J, Adams LH, Maier HJ. 2019. The Porcine
875 Deltacoronavirus Replication Organelle Comprises Double-Membrane Vesicles and
876 Zippered Endoplasmic Reticulum with Double-Membrane Spherules. Viruses 11:E1030.

877 7. Snijder EJ, Limpens RWAL, de Wilde AH, de Jong AWM, Zevenhoven-Dobbe JC, Maier
878 HJ, Faas FFGA, Koster AJ, Bárcena M. 2020. A unifying structural and functional model

879 of the coronavirus replication organelle: Tracking down RNA synthesis. PLoS Biol
880 18:e3000715.

881 8. Wolff G, Limpens RWAL, Zevenhoven-Dobbe JC, Laugks U, Zheng S, de Jong AWM,
882 Koning RI, Agard DA, Grünewald K, Koster AJ, Snijder EJ, Bárcena M. 2020. A
883 molecular pore spans the double membrane of the coronavirus replication organelle.
884 Science 369:1395–1398.

885 9. Kanjanahaluethai A, Chen Z, Jukneliene D, Baker SC. 2007. Membrane topology of murine
886 coronavirus replicase nonstructural protein 3. Virology 361:391–401.

887 10. Oostra M, te Lintelo EG, Deijs M, Verheije MH, Rottier PJM, de Haan C a. M. 2007.
888 Localization and membrane topology of coronavirus nonstructural protein 4: involvement
889 of the early secretory pathway in replication. J Virol 81:12323–12336.

890 11. Tooze J, Tooze S, Warren G. 1984. Replication of coronavirus MHV-A59 in sac- cells:
891 determination of the first site of budding of progeny virions. Eur J Cell Biol 33:281–293.

892 12. Goldsmith CS, Tatti KM, Ksiazek TG, Rollin PE, Comer JA, Lee WW, Rota PA, Bankamp
893 B, Bellini WJ, Zaki SR. 2004. Ultrastructural characterization of SARS coronavirus. Emerg
894 Infect Dis 10:320–326.

895 13. Stertz S, Reichelt M, Spiegel M, Kuri T, Martínez-Sobrido L, García-Sastre A, Weber F,
896 Kochs G. 2007. The intracellular sites of early replication and budding of SARS-
897 coronavirus. Virology 361:304–315.

898 14. Ghosh S, Dellibovi-Ragheb TA, Kerviel A, Pak E, Qiu Q, Fisher M, Takvorian PM, Bleck
899 C, Hsu VW, Fehr AR, Perlman S, Achar SR, Straus MR, Whittaker GR, de Haan CAM,
900 Kehrl J, Altan-Bonnet G, Altan-Bonnet N. 2020. β-Coronaviruses Use Lysosomes for
901 Egress Instead of the Biosynthetic Secretory Pathway. Cell 183:1520-1535.e14.

902 15. Fung TS, Liu DX. 2018. Post-translational modifications of coronavirus proteins: roles and
903 function. Future Virol 13:405–430.

904 16. Delmas B, Laude H. 1990. Assembly of coronavirus spike protein into trimers and its role
905 in epitope expression. J Virol 64:5367–5375.

906 17. Belouzard S, Chu VC, Whittaker GR. 2009. Activation of the SARS coronavirus spike
907 protein via sequential proteolytic cleavage at two distinct sites. Proc Natl Acad Sci U S A
908 106:5871–5876.

909 18. Millet JK, Whittaker GR. 2014. Host cell entry of Middle East respiratory syndrome
910 coronavirus after two-step, furin-mediated activation of the spike protein. Proc Natl Acad
911 Sci U S A 111:15214–15219.

912 19. Schoeman D, Fielding BC. 2019. Coronavirus envelope protein: current knowledge. Virol J
913 16:69.

914 20. Boson B, Legros V, Zhou B, Siret E, Mathieu C, Cosset F-L, Lavillette D, Denolly S. 2021.
915 The SARS-CoV-2 envelope and membrane proteins modulate maturation and retention of
916 the spike protein, allowing assembly of virus-like particles. J Biol Chem 296:100111.

917 21. Liao Y, Fung TS, Huang M, Fang SG, Zhong Y, Liu DX. 2013. Upregulation of
918 CHOP/GADD153 during coronavirus infectious bronchitis virus infection modulates
919 apoptosis by restricting activation of the extracellular signal-regulated kinase pathway. J
920 Virol 87:8124–8134.

921 22. Fung TS, Liao Y, Liu DX. 2014. The endoplasmic reticulum stress sensor IRE1α protects
922 cells from apoptosis induced by the coronavirus infectious bronchitis virus. J Virol
923 88:12752–12764.

924 23. Versteeg GA, van de Nes PS, Bredenbeek PJ, Spaan WJM. 2007. The coronavirus spike
925 protein induces endoplasmic reticulum stress and upregulation of intracellular chemokine
926 mRNA concentrations. J Virol 81:10981–10990.

927 24. Xue M, Fu F, Ma Y, Zhang X, Li L, Feng L, Liu P. 2018. The PERK Arm of the Unfolded
928 Protein Response Negatively Regulates Transmissible Gastroenteritis Virus Replication by
929 Suppressing Protein Translation and Promoting Type I Interferon Production. J Virol
930 92:e00431-18.

931 25. Favreau DJ, Desforges M, St-Jean JR, Talbot PJ. 2009. A human coronavirus OC43 variant
932 harboring persistence-associated mutations in the S glycoprotein differentially induces the
933 unfolded protein response in human neurons as compared to wild-type virus. Virology
934 395:255–267.

935 26. Tang BSF, Chan K-H, Cheng VCC, Woo PCY, Lau SKP, Lam CCK, Chan T-L, Wu AKL,
936 Hung IFN, Leung S-Y, Yuen K-Y. 2005. Comparative host gene transcription by

937 microarray analysis early after infection of the Huh7 cell line by severe acute respiratory
938 syndrome coronavirus and human coronavirus 229E. J Virol 79:6180–6193.

939 27. Chan C-P, Siu K-L, Chin K-T, Yuen K-Y, Zheng B, Jin D-Y. 2006. Modulation of the
940 unfolded protein response by the severe acute respiratory syndrome coronavirus spike
941 protein. J Virol 80:9279–9287.

942 28. Yeung Y-S, Yip C-W, Hon C-C, Chow KYC, Ma ICM, Zeng F, Leung FCC. 2008.
943 Transcriptional profiling of Vero E6 cells over-expressing SARS-CoV S2 subunit: insights
944 on viral regulation of apoptosis and proliferation. Virology 371:32–43.

945 29. Bechill J, Chen Z, Brewer JW, Baker SC. 2008. Coronavirus infection modulates the
946 unfolded protein response and mediates sustained translational repression. J Virol 82:4492–
947 4501.

948 30. Siu K-L, Chan C-P, Kok K-H, Woo PC-Y, Jin D-Y. 2014. Comparative analysis of the
949 activation of unfolded protein response by spike proteins of severe acute respiratory
950 syndrome coronavirus and human coronavirus HKU1. Cell Biosci 4:3.

951 31. Ye Z, Wong CK, Li P, Xie Y. 2008. A SARS-CoV protein, ORF-6, induces caspase-3
952 mediated, ER stress and JNK-dependent apoptosis. Biochim Biophys Acta 1780:1383–
953 1387.

954 32. Minakshi R, Padhan K, Rani M, Khan N, Ahmad F, Jameel S. 2009. The SARS
955 Coronavirus 3a protein causes endoplasmic reticulum stress and induces ligand-
956 independent downregulation of the type 1 interferon receptor. PloS One 4:e8342.

957 33. Sung S-C, Chao C-Y, Jeng K-S, Yang J-Y, Lai MMC. 2009. The 8ab protein of SARS-
958 CoV is a luminal ER membrane-associated protein and induces the activation of ATF6.
959 Virology 387:402–413.

960 34. Slaine PD, Kleer M, Duguay BA, Pringle ES, Kadijk E, Ying S, Balgi A, Roberge M,
961 McCormick C, Khaperskyy DA. 2021. Thiopurines activate an antiviral unfolded protein
962 response that blocks influenza A virus glycoprotein accumulation. J Virol JVI.00453-21.

963 35. Lepage GA. 1960. Incorporation of 6-thioguanine into nucleic acids. Cancer Res 20:403–
964 408.

965 36. Brem R, Karran P. 2012. Oxidation-mediated DNA cross-linking contributes to the toxicity
966 of 6-thioguanine in human cells. Cancer Res 72:4787–4795.

967 37. Shin J-Y, Wey M, Umutesi HG, Sun X, Simecka J, Heo J. 2016. Thiopurine Prodrugs
968 Mediate Immunosuppressive Effects by Interfering with Rac1 Protein Function. J Biol
969 Chem 291:13699–13714.

970 38. de Boer NKH, van Bodegraven AA, Jharap B, de Graaf P, Mulder CJJ. 2007. Drug Insight:
971 pharmacology and toxicity of thiopurine therapy in patients with IBD. Nat Clin Pract
972 Gastroenterol Hepatol 4:686–694.

973 39. Chou C-Y, Chien C-H, Han Y-S, Prebanda MT, Hsieh H-P, Turk B, Chang G-G, Chen X.
974 2008. Thiopurine analogues inhibit papain-like protease of severe acute respiratory
975 syndrome coronavirus. Biochem Pharmacol 75:1601–1609.

976 40. Chen X, Chou C-Y, Chang G-G. 2009. Thiopurine analogue inhibitors of severe acute
977 respiratory syndrome-coronavirus papain-like protease, a deubiquitinating and
978 deISGylating enzyme. Antivir Chem Chemother 19:151–156.

979 41. Cheng K-W, Cheng S-C, Chen W-Y, Lin M-H, Chuang S-J, Cheng I-H, Sun C-Y, Chou C-
980 Y. 2015. Thiopurine analogs and mycophenolic acid synergistically inhibit the papain-like
981 protease of Middle East respiratory syndrome coronavirus. Antiviral Res 115:9–16.

982 42. Swaim CD, Perng Y-C, Zhao X, Canadeo LA, Harastani HH, Darling TL, Boon ACM,
983 Lenschow DJ, Huibregtse JM. 2020. 6-Thioguanine blocks SARS-CoV-2 replication by
984 inhibition of PLpro protease activities. BioRxiv Prepr Serv Biol 2020.07.01.183020.

985 43. Tiede I, Fritz G, Strand S, Poppe D, Dvorsky R, Strand D, Lehr HA, Wirtz S, Becker C,
986 Atreya R, Mudter J, Hildner K, Bartsch B, Holtmann M, Blumberg R, Walczak H, Iven H,
987 Galle PR, Ahmadian MR, Neurath MF. 2003. CD28-dependent Rac1 activation is the
988 molecular target of azathioprine in primary human CD4+ T lymphocytes. J Clin Invest
989 111:1133–1145.

990 44. Poppe D, Tiede I, Fritz G, Becker C, Bartsch B, Wirtz S, Strand D, Tanaka S, Galle PR,
991 Bustelo XR, Neurath MF. 2006. Azathioprine suppresses ezrin-radixin-moesin-dependent T
992 cell-APC conjugation through inhibition of Vav guanosine exchange activity on Rac
993 proteins. J Immunol Baltim Md 1950 176:640–651.

994 45. Schultz DC, Johnson RM, Ayyanathan K, Miller J, Whig K, Kamalia B, Dittmar M,
995 Weston S, Hammond HL, Dillen C, Ardanuy J, Taylor L, Lee JS, Li M, Lee E, Shoffler C,
996 Petucci C, Constant S, Ferrer M, Thaiss CA, Frieman MB, Cherry S. 2022. Pyrimidine

997 inhibitors synergize with nucleoside analogues to block SARS-CoV-2. Nature
998 https://doi.org/10.1038/s41586-022-04482-x.

999 46. Al-Beltagi S, Preda CA, Goulding LV, James J, Pu J, Skinner P, Jiang Z, Wang BL, Yang
1000 J, Banyard AC, Mellits KH, Gershkovich P, Hayes CJ, Nguyen-Van-Tam J, Brown IH, Liu
1001 J, Chang K-C. 2021. Thapsigargin Is a Broad-Spectrum Inhibitor of Major Human
1002 Respiratory Viruses: Coronavirus, Respiratory Syncytial Virus and Influenza A Virus.
1003 Viruses 13:234.

1004 47. Al-Beltagi S, Goulding LV, Chang DKE, Mellits KH, Hayes CJ, Gershkovich P, Coleman
1005 CM, Chang K-C. 2021. Emergent SARS-CoV-2 variants: comparative replication dynamics
1006 and high sensitivity to thapsigargin. Virulence 12:2946–2956.

1007 48. Shaban MS, Müller C, Mayr-Buro C, Weiser H, Meier-Soelch J, Albert BV, Weber A,
1008 Linne U, Hain T, Babayev I, Karl N, Hofmann N, Becker S, Herold S, Schmitz ML,
1009 Ziebuhr J, Kracht M. 2021. Multi-level inhibition of coronavirus replication by chemical
1010 ER stress. Nat Commun 12:5536.

1011 49. Santos-Beneit F, Raškevičius V, Skeberdis VA, Bordel S. 2021. A metabolic modeling
1012 approach reveals promising therapeutic targets and antiviral drugs to combat COVID-19.
1013 Sci Rep 11:11982.

1014 50. Oostra M, de Haan C a. M, de Groot RJ, Rottier PJM. 2006. Glycosylation of the severe
1015 acute respiratory syndrome coronavirus triple-spanning membrane proteins 3a and M. J
1016 Virol 80:2326–2336.

1017 51. Tarentino AL, Trimble RB, Plummer TH. 1989. Enzymatic approaches for studying the
1018 structure, synthesis, and processing of glycoproteins. Methods Cell Biol 32:111–139.

1019 52. Tian W, Li D, Zhang N, Bai G, Yuan K, Xiao H, Gao F, Chen Y, Wong CCL, Gao GF.
1020 2021. O-glycosylation pattern of the SARS-CoV-2 spike protein reveals an "O-Follow-N"
1021 rule. Cell Res https://doi.org/10.1038/s41422-021-00545-2.

1022 53. Sanda M, Morrison L, Goldman R. 2021. N- and O-Glycosylation of the SARS-CoV-2
1023 Spike Protein. Anal Chem 93:2003–2009.

1024 54. Shajahan A, Supekar NT, Gleinich AS, Azadi P. 2020. Deducing the N- and O-
1025 glycosylation profile of the spike protein of novel coronavirus SARS-CoV-2. Glycobiology
1026 30:981–988.

1027 55. Tannous BA, Kim D-E, Fernandez JL, Weissleder R, Breakefield XO. 2005. Codon-
1028 optimized Gaussia luciferase cDNA for mammalian gene expression in culture and in vivo.
1029 Mol Ther J Am Soc Gene Ther 11:435–443.

1030 56. Helms JB, Rothman JE. 1992. Inhibition by brefeldin A of a Golgi membrane enzyme that
1031 catalyses exchange of guanine nucleotide bound to ARF. Nature 360:352–354.

1032 57. Donaldson JG, Finazzi D, Klausner RD. 1992. Brefeldin A inhibits Golgi membrane-
1033 catalysed exchange of guanine nucleotide onto ARF protein. Nature 360:350–352.

1034 58. Crawford KHD, Eguia R, Dingens AS, Loes AN, Malone KD, Wolf CR, Chu HY, Tortorici
1035 MA, Veesler D, Murphy M, Pettie D, King NP, Balazs AB, Bloom JD. 2020. Protocol and

1036 Reagents for Pseudotyping Lentiviral Particles with SARS-CoV-2 Spike Protein for
1037 Neutralization Assays. Viruses 12:E513.

1038 59. Hu J, Gao Q, He C, Huang A, Tang N, Wang K. 2020. Development of cell-based
1039 pseudovirus entry assay to identify potential viral entry inhibitors and neutralizing
1040 antibodies against SARS-CoV-2. Genes Dis 7:551–557.

1041 60. Ou X, Liu Y, Lei X, Li P, Mi D, Ren L, Guo L, Guo R, Chen T, Hu J, Xiang Z, Mu Z, Chen
1042 X, Chen J, Hu K, Jin Q, Wang J, Qian Z. 2020. Characterization of spike glycoprotein of
1043 SARS-CoV-2 on virus entry and its immune cross-reactivity with SARS-CoV. Nat
1044 Commun 11:1620.

1045 61. Ujike M, Taguchi F. 2015. Incorporation of spike and membrane glycoproteins into
1046 coronavirus virions. Viruses 7:1700–1725.

1047 62. Nie J, Li Q, Wu J, Zhao C, Hao H, Liu H, Zhang L, Nie L, Qin H, Wang M, Lu Q, Li X,
1048 Sun Q, Liu J, Fan C, Huang W, Xu M, Wang Y. 2020. Establishment and validation of a
1049 pseudovirus neutralization assay for SARS-CoV-2. Emerg Microbes Infect 9:680–686.

1050 63. Schmidt F, Weisblum Y, Muecksch F, Hoffmann H-H, Michailidis E, Lorenzi JCC,
1051 Mendoza P, Rutkowska M, Bednarski E, Gaebler C, Agudelo M, Cho A, Wang Z,
1052 Gazumyan A, Cipolla M, Caskey M, Robbiani DF, Nussenzweig MC, Rice CM,
1053 Hatziioannou T, Bieniasz PD. 2020. Measuring SARS-CoV-2 neutralizing antibody activity
1054 using pseudotyped and chimeric viruses. J Exp Med 217:e20201181.

1055 64. Yin Y, Chen S, Hakim MS, Wang W, Xu L, Dang W, Qu C, Verhaar AP, Su J, Fuhler GM,
1056 Peppelenbosch MP, Pan Q. 2018. 6-Thioguanine inhibits rotavirus replication through
1057 suppression of Rac1 GDP/GTP cycling. Antiviral Res 156:92–101.

1058 65. Palsuledesai CC, Surviladze Z, Waller A, Miscioscia TF, Guo Y, Wu Y, Strouse J, Romero
1059 E, Salas VM, Curpan R, Young S, Carter M, Foutz T, Galochkina Z, Ames H, Haynes MK,
1060 Edwards BS, Nicolotti O, Luo L, Ursu O, Bologa CG, Oprea TI, Wandinger-Ness A, Sklar
1061 LA. 2018. Activation of Rho Family GTPases by Small Molecules. ACS Chem Biol
1062 13:1514–1524.

1063 66. Blight KJ, McKeating JA, Rice CM. 2002. Highly permissive cell lines for subgenomic and
1064 genomic hepatitis C virus RNA replication. J Virol 76:13001–13014.

1065 67. Johnston BP, Pringle ES, McCormick C. 2019. KSHV activates unfolded protein response
1066 sensors but suppresses downstream transcriptional responses to support lytic replication.
1067 PLoS Pathog 15:e1008185.

1068 68. Mendoza EJ, Manguiat K, Wood H, Drebot M. 2020. Two Detailed Plaque Assay Protocols
1069 for the Quantification of Infectious SARS-CoV-2. Curr Protoc Microbiol 57:ecpmc105.

1070 69. Craig N, Fletcher SL, Daniels A, Newman C, O'Shea M, Warr A, Tait-Burkard C. 2021.
1071 Direct lysis RT-qPCR of SARS-CoV-2 in cell culture supernatant allows for fast and
1072 accurate quantification of virus, opening a vast array of applications. preprint.
1073 Microbiology.

1074 70. Wrapp D, Wang N, Corbett KS, Goldsmith JA, Hsieh C-L, Abiona O, Graham BS,
1075 McLellan JS. 2020. Cryo-EM structure of the 2019-nCoV spike in the prefusion
1076 conformation. Science 367:1260–1263.

1077 71. Pallesen J, Wang N, Corbett KS, Wrapp D, Kirchdoerfer RN, Turner HL, Cottrell CA,
1078 Becker MM, Wang L, Shi W, Kong W-P, Andres EL, Kettenbach AN, Denison MR,
1079 Chappell JD, Graham BS, Ward AB, McLellan JS. 2017. Immunogenicity and structures of
1080 a rationally designed prefusion MERS-CoV spike antigen. Proc Natl Acad Sci U S A
1081 114:E7348–E7357.

1082 72. Kirchdoerfer RN, Wang N, Pallesen J, Wrapp D, Turner HL, Cottrell CA, Corbett KS,
1083 Graham BS, McLellan JS, Ward AB. 2018. Stabilized coronavirus spikes are resistant to
1084 conformational changes induced by receptor recognition or proteolysis. Sci Rep 8:15701.

1085 73. Duguay BA, Herod A, Pringle ES, Monro SMA, Hetu M, Cameron CG, McFarland SA,
1086 McCormick C. 2022. Photodynamic Inactivation of Human Coronaviruses. Viruses 14:110.

1087

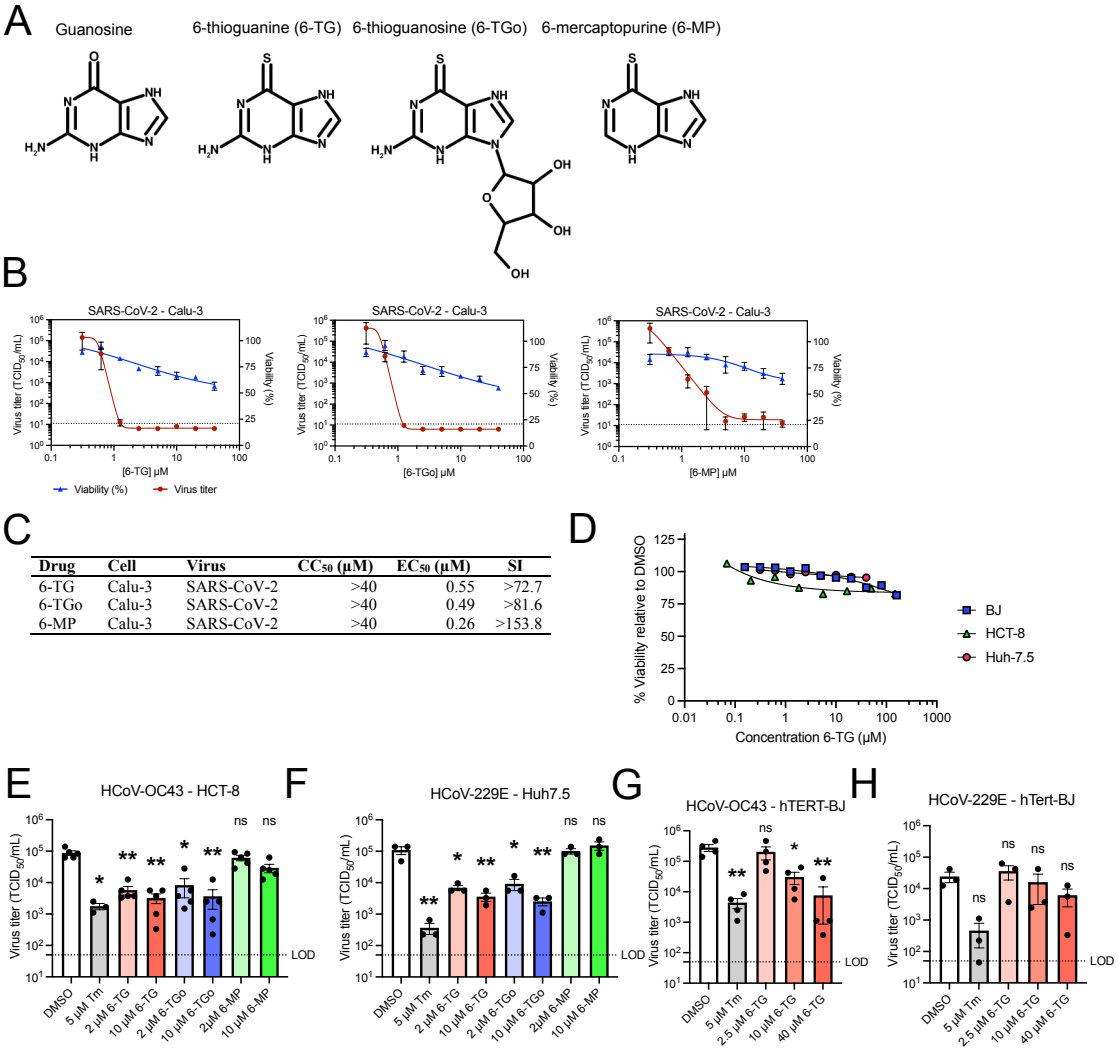

Drug	Cell	Virus	CC_{50} (µM)	EC_{50} (µM)	SI
6-TG	Calu-3	SARS-CoV-2	>40	0.55	>72.7
6-TGo	Calu-3	SARS-CoV-2	>40	0.49	>81.6
6-MP	Calu-3	SARS-CoV-2	>40	0.26	>153.8

Figure 1. Thiopurines 6-thioguanine and 6-thioguanosine inhibit coronavirus replication. (A) Structures of thiopurines used this study in comparison to Guanosine. **(B)** Calu-3 cells were infected with SARS-CoV-2 at an MOI of 0.1 then treated with 6-thioguanine (6-TG), 6-thioguanosine (6-TGo), or 6-mercaptopurine (6-MP). Supernatant was harvested after 48 h, and stored at -80°C until titering on Vero'76 cells. Mock-infected cells were similarly treated with 6-TG, 6-TGo, 6-MP, or DMSO vehicle control for 48 h before testing cell viability with CellTiter 96 AQueous One (n=3 ± SEM). **(C)** Summary table of Cellular Cytotoxicity (CC_{50}), Effective concentration (EC_{50}), and Selectivity Index (SI) calculated for (A-C). **(D)** Alamar Blue cell viability assay of hTert-BJ, HCT-8, and Huh-7.5 cells treated with 6-TG (n=3±SEM).**(E)** TCID assays for HCoV-OC43 infected HCT-8 cells and **(F)** HCoV-229E infected Huh-7.5. Cells were infected with an MOI of 0.1 then treated with 6-TG, 6-TGo, 6-MP, or DMSO (n=3 ± SEM, statistical significance was determined by one-way ANOVA). **(F)** hTERT-BJ cells were infected with HCoV-OC43 or HCoV-229E at an MOI of 0.1 and treated with 6-TG, Tm, or DMSO. Supernatant was harvested after 23 h and stored at -80°C before titering on BHK-21 or Huh7.5 (n=3-4 ± SEM, statistical significance was determined by one-way ANOVA). **(G)** hTERT-BJ cells were infected with HCoV-OC43 or **(H)** HCoV-229E at an MOI of 0.1 and treated with 6-TG, Tm, or DMSO. Supernatant was harvested after 23 h and stored at -80°C before titering on BHK-21 or Huh7.5 (n=3-4 ± SEM, statistical significance was determined by one-way ANOVA). LoD = Limit of Detection for virus titer. (*, $p<0.05$; **, $p<0.01$; ns, non-significant)

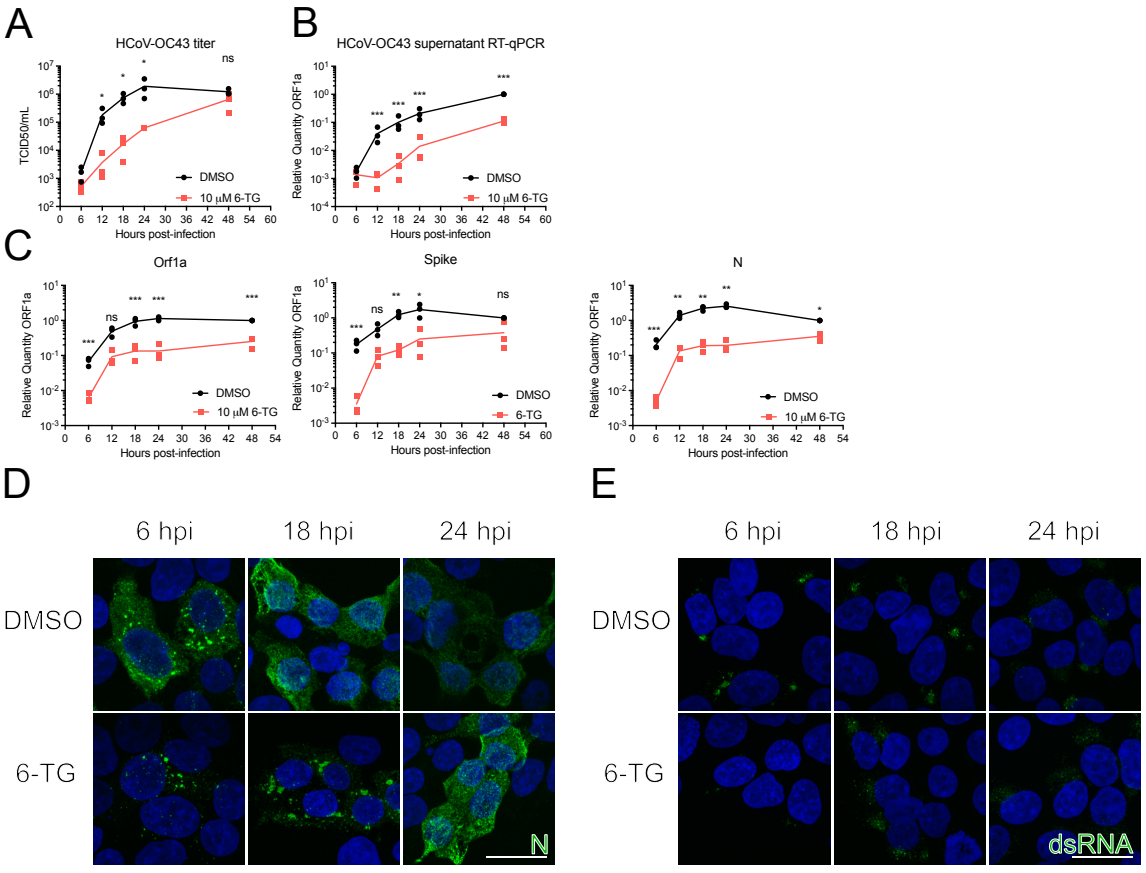

Figure 2. 6-TG reduces CoV protein and mRNA accumulation. (A-C) 293T cells were infected with HCoV-OC43 at an MOI of 0.1 then treated with 10 µM 6-TG or DMSO vehicle control. Supernatant and total RNA from the cells were harvested at the times indicated and stored at -80°C until **(A)** titering on BHK-21 or **(B)** quantification of viral genomes by RT-qPCR. Cell monolayers were harvested for **(C)** RT-qPCR analysis of viral RNA accumulation (n=3 statistical significance was determined by paired ratio t test; *, $p<0.05$; **, $p<0.01$; ns, non-significant) **(D)** 293T cells were grown on coverslips then infected with HCoV-OC43 and treated with 6-TG as in (A), then fixed and immunostained for N or **(E)** dsRNA. Nuclei are counterstained with Hoechst. Scale bar = 20 µm.

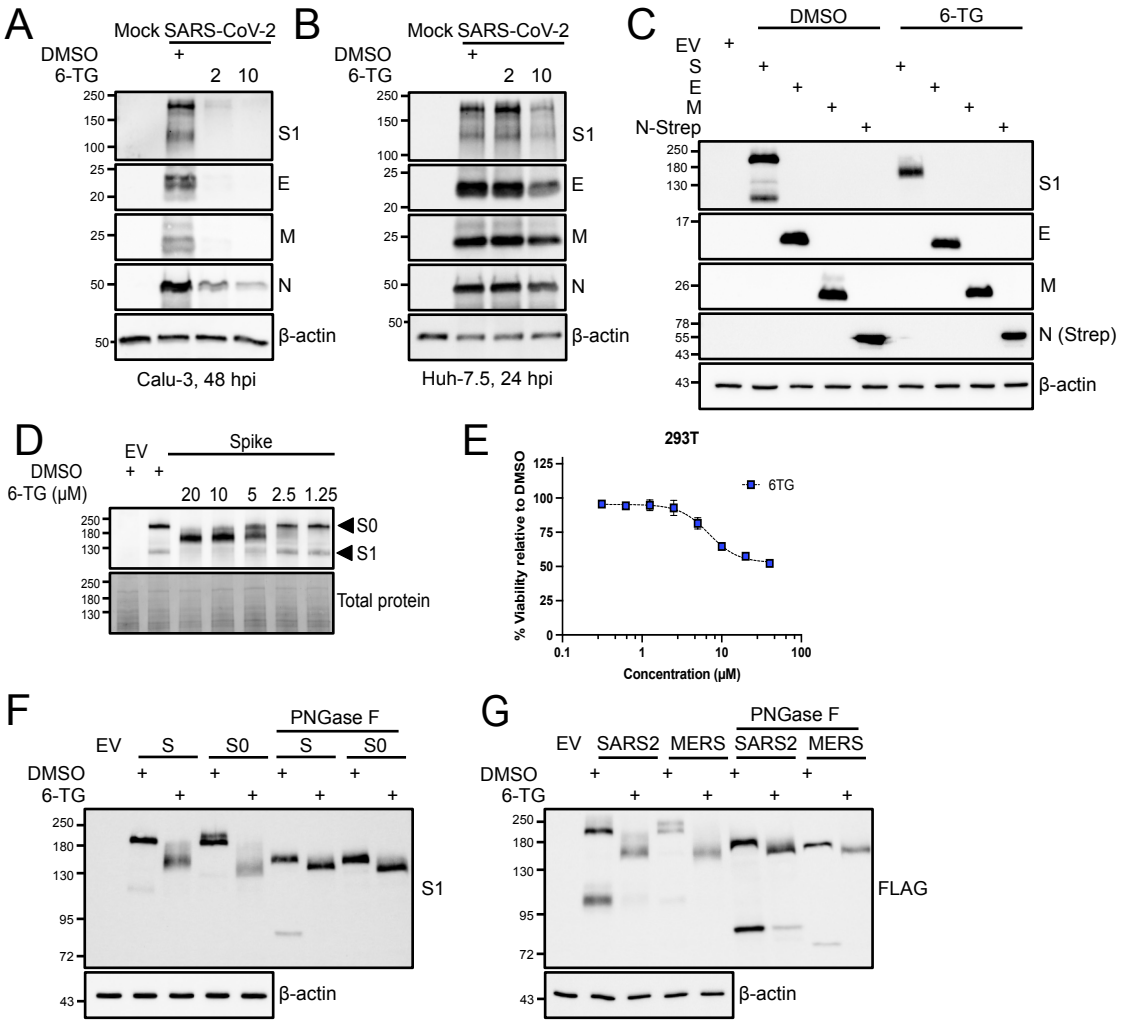

Figure 3. 6-TG inhibits Spike glycosylation and cleavage. **(A)** Calu-3 cells were infected with SARS-CoV-2 at an MOI of 7, then treated with 6-TG or DMSO. Lysates were harvested 48 h after transfection and were probed by western blotting as indicated. Concentrations in legend are in μM. **(B)** Huh-7.5 cells were infected with SARS-CoV-2 at an MOI of 5, then treated with 6-TG or DMSO. Lysates were harvested 48 h after transfection and were probed by western blotting as indicated. Concentrations in legend are in μM. **(C)** 293T cells were transfected with SARS-CoV-2 S, M, Envelope (E), Nucleoprotein (N) with a C-terminal 2xStrep tag, or EV then treated with 10 μM 6-TG or DMSO vehicle control. Lysates were harvested 24 h after transfection and probed by western blotting as indicated. **(D)** 293T cells were transfected with SARS-CoV-2 Spike or EV then treated with 6-TG or DMSO vehicle control. Lysates were harvested 24 h after transfection and were probed by western blotting as indicated. Concentrations in legend are in μM. **(E)** Alamar Blue cell viability assay of 6-TG treated 293T cells (n=3±SEM). **(F)** 293T cells were transfected with SARS-CoV-2 Spike (S), a Spike mutant lacking the Furin cleavage site between S1 and S2 (S0), or EV then treated with 10 μM 6-TG or DMSO vehicle control. Lysates were harvested 24 h after transfection, treated with PNGase F to remove N-linked glycans, and probed by western blotting as indicated. **(G)** as in (C) except 293T cells were transfected with C-terminal FLAG-tagged Spike (S-FL) or HCoV-MERS Spike (MERS).

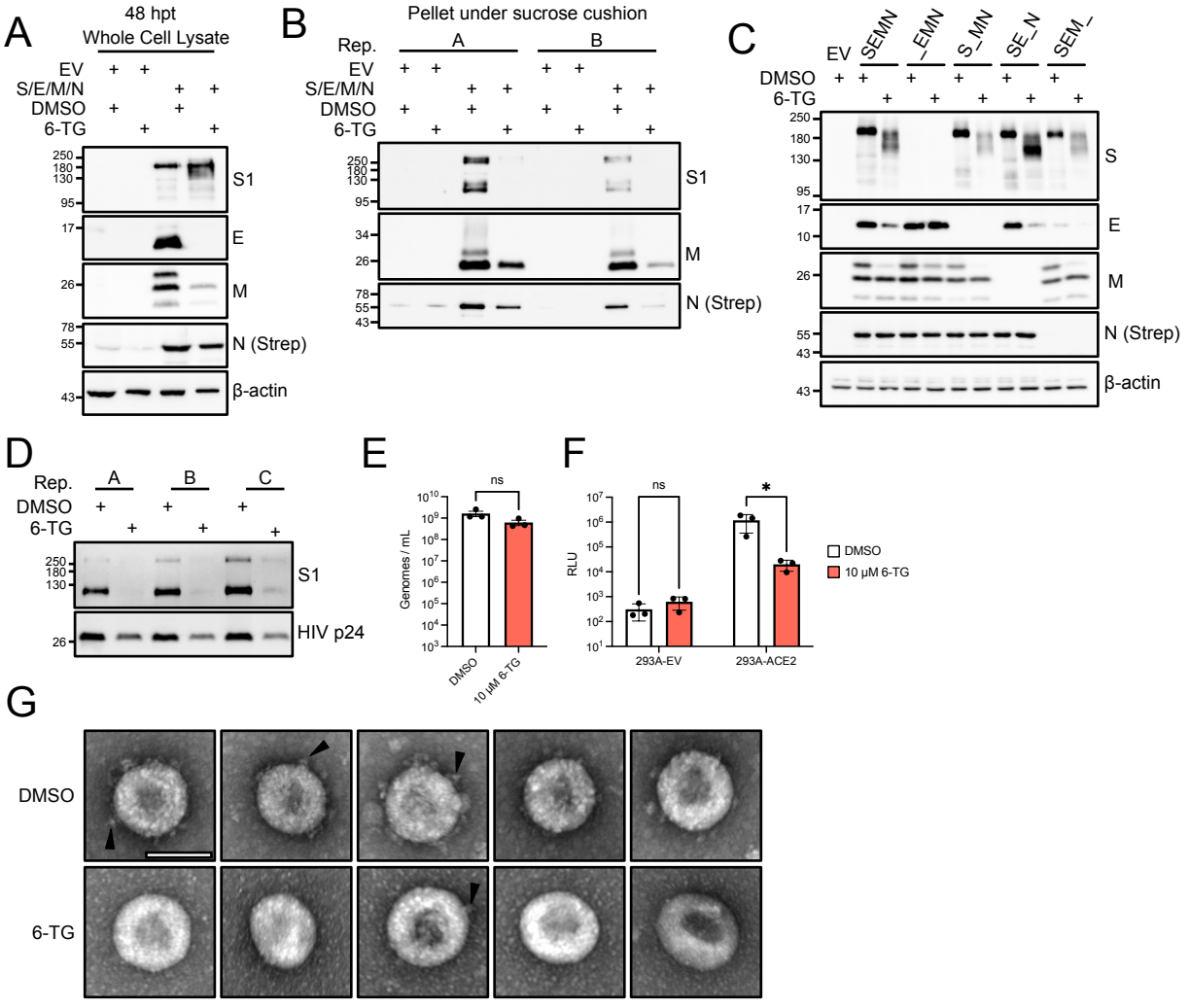

Figure 4. 6-TG stimulates an assembly defect and inhibits Spike virion incorporation. (A) 293T cells were transfected with equal quantities of SARS-CoV-2 S, M, E, and N or empty vector (EV) then treated with 10 µM 6-TG or DMSO vehicle control. Lysates were harvested 48 h after transfection and probed by western blotting as indicated. **(B)** Virus-like particles from supernatants of cells transfected in (B) were concentrated by ultracentrifugation through a 20% sucrose cushion, resuspended in PBS, then harvested with an equal volume of 2x Leammli buffer. Samples from two independent lentivirus preparations were probed by western blotting as indicated. **(C)** 293T cells were transfected with S, E, M, and N in a 1:2:2:1 ratio, substituting one of the structural proteins for EV as indicated, treated with 6-TG or DMSO then processed as in (A). **(D)** SARS-CoV-2 Spike pseudotyped, luciferase-expressing lentivirus particles were concentrated by ultracentrifugation through a 20% sucrose cushion, resuspended in PBS, then harvested with an equal volume of 2x Leammli buffer. Samples from three independent lentivirus preparations were probed by western blotting as indicated. **(E)** Genomes from three independent lentivirus preparations were quantified by RT-qPCR (n=3, statistical significance was determined by paired t-test; ns, non-significant). **(F)** 293A cells stably expressing ACE2 or and empty vector control were transduced with lentivirus from three independent preparations. After 24 h, lysates were harvested and measured for luciferase activity (n=3, statistical significance was determined by two-way ANOVA; *, $p<0.05$; ns, non-significant). **(G)** 293A cells were infected HCoV-OC43 at an MOI of 0.1 =, then treated with 6-TG or DMSO. Supernatants were concentrated as in (C), before virions were fixed and imaged and imaged by TEM with negative staining. Five virions from both 6-TG- and DMSO-treated samples are shown at 150,000 X magnification. Scale bar = 100 nm. Arrowhead indicates examples of Spike protein extending from virion.

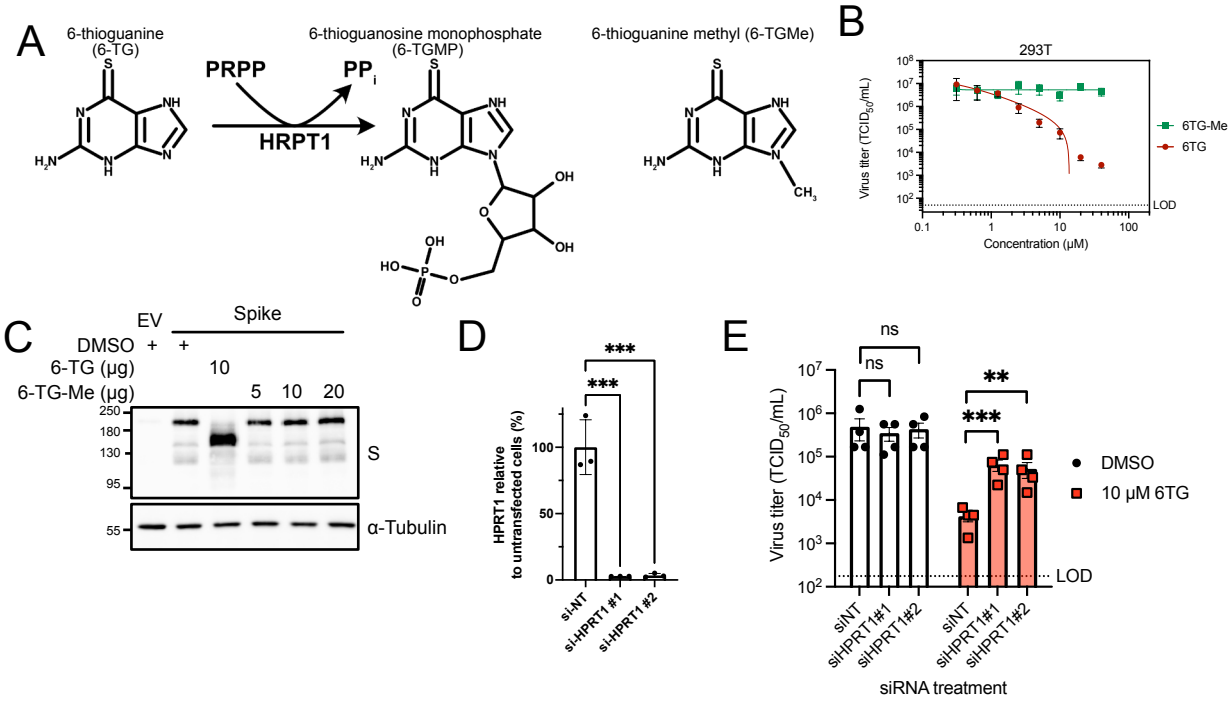

Figure 5. 6-TG inhibits Spike maturation through GTPase inhibition. (A) 6-TG is conjugated to phosphoribosyl diphosphate (PRPP) by HPRT1 to form 6-TG monophosphate. 6-TG methylated at the N9 nitrogen was designed to be resistant to processing by HPRT1. **(B)** 293T cells were infected with HCoV-OC43 at an MOI of 0.1 then treated with 6-TG or 6-TG-Me. Supernatant was harvested at the times indicated and stored at -80°C until titering on BHK cells. (n=3 statistical significance was determined by paired ratio t test; *, p<0.05; **, p<0.01; ns, non-significant). **(C)** 293T cells were transfected with SARS-CoV-2 Spike or an empty vector control then treated with 6-TG, 6-TG-Me, or DMSO vehicle control. Lysates were harvested 24 h after transfection, treated with PNGase F to remove N-linked glycans, and probed by western blotting as indicated. **(D)** 293T cells were reversed transfected with siRNA and total RNA was harvested after 48 h. HPRT1mRNA abundance was measured by RT-qPCR (n=3, ±SEM statistical significance was determined by one way ANOVA; ***, p<0.001). **(E)** As in D but cells were infected with HCoV-OC43 at an MOI of 0.1 24 h after siRNA treatment and supernatant was harvested and titered as in **(B)** (n=4 ±SEM statistical significance was determined by paired ratio t test; **, p<0.01; ***, p<0.001; ns, non-significant).

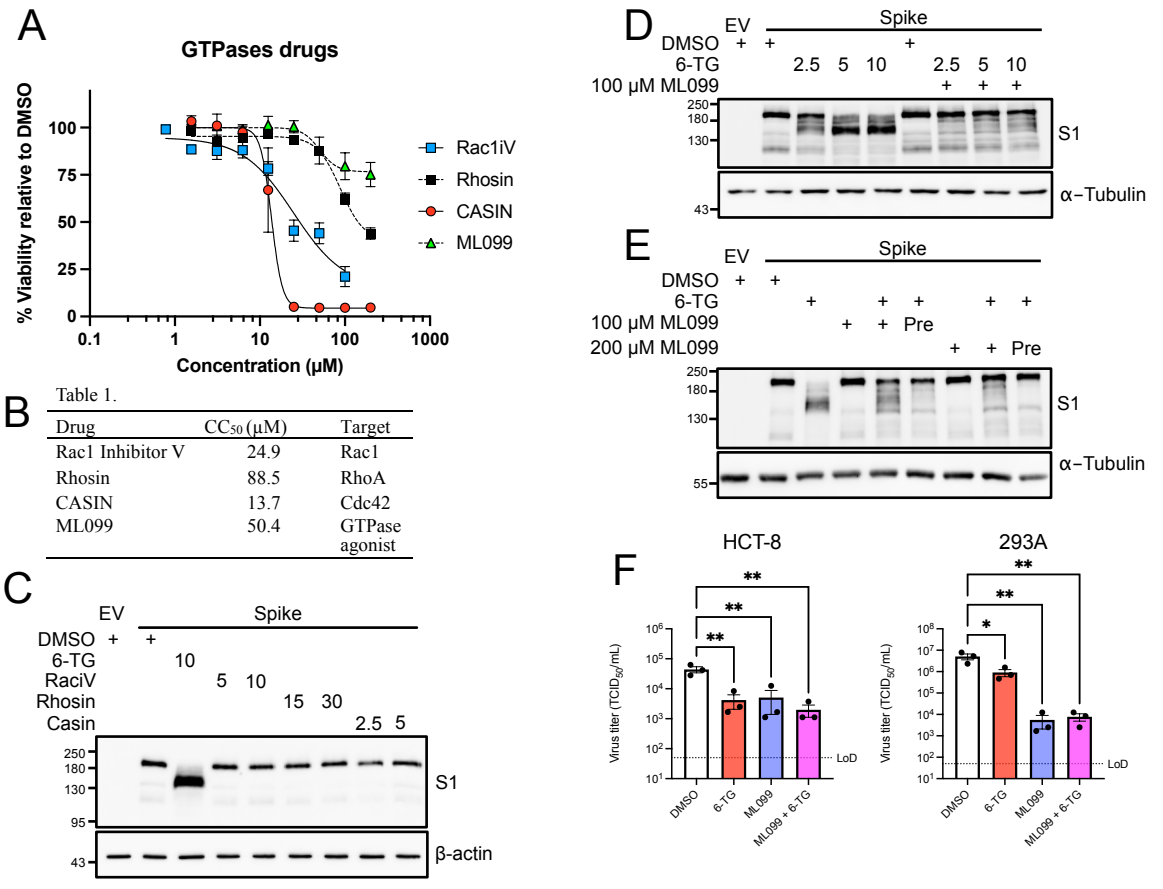

Figure 6. 6-TG inhibits Spike maturation through GTPase inhibition. (A) Alamar Blue cell viability assay of 293T cells treated Rac1 Inhibitor V (Rac1iV), Rhosin, CASIN, or ML099 (n=3±SEM). **(B)** Summary table of Cellular Cytotoxicity (CC_{50}) and inhibitor target of compounds tested in (A). **(C)** 293T cells were transfected with SARS-CoV-2 Spike or an empty vector control (EV) then treated with 6-TG, GTPase inhibitors, or DMSO vehicle control. Concentrations in legend are in μM. Lysates were harvested 24 h after transfection and were probed by western blotting as indicated. **(D)** 293T cells were transfected with plasmids encoding Spike or EV then co-treated with 6-TG, 100 μM ML099 GTPase agonist, or DMSO. Lysates were harvested 24 h after transfection and were probed by western blotting as indicated. Concentrations in legend are in μM **(E)** as in (D) except some samples were pre-treated (Pre) for 4 h with ML099. **(F)** HCT-8 and 293A were infected with an MOI of ~0.1 then treated with 10 μM 6-TG or DMSO vehicle control. After 24 h, the supernatants was harvested and stored at -80°C until titering on BHK-21 (n=3 ± SEM, statistical significance was determined by one-way ANOVA; *, $p<0.05$; **, $p<0.01$; ns, non-significant). LoD = Limit of Detection for virus titer.

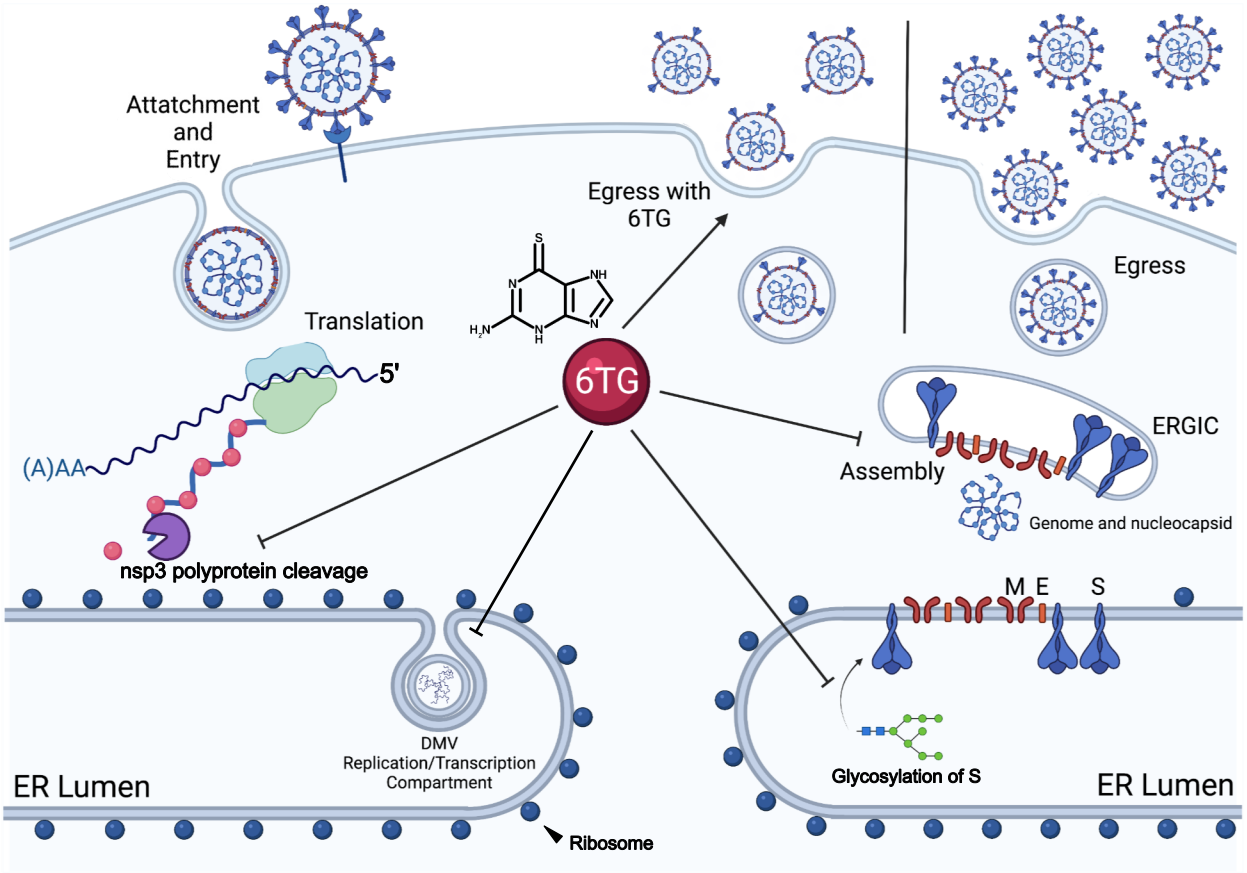

Figure 7. 6-TG inhibits multiple essential steps in virus replication and assembly. 6-TG inhibits nsp3, delaying formation of replication compartments and reducing accumulation of viral RNA. 6-TG also inhibits normal glycosylation of Spike, which fails to be properly packaged in egressing virions. As a result, the total number of virions released from infected cells is reduced and those that are released have fewer Spikes on their surface.

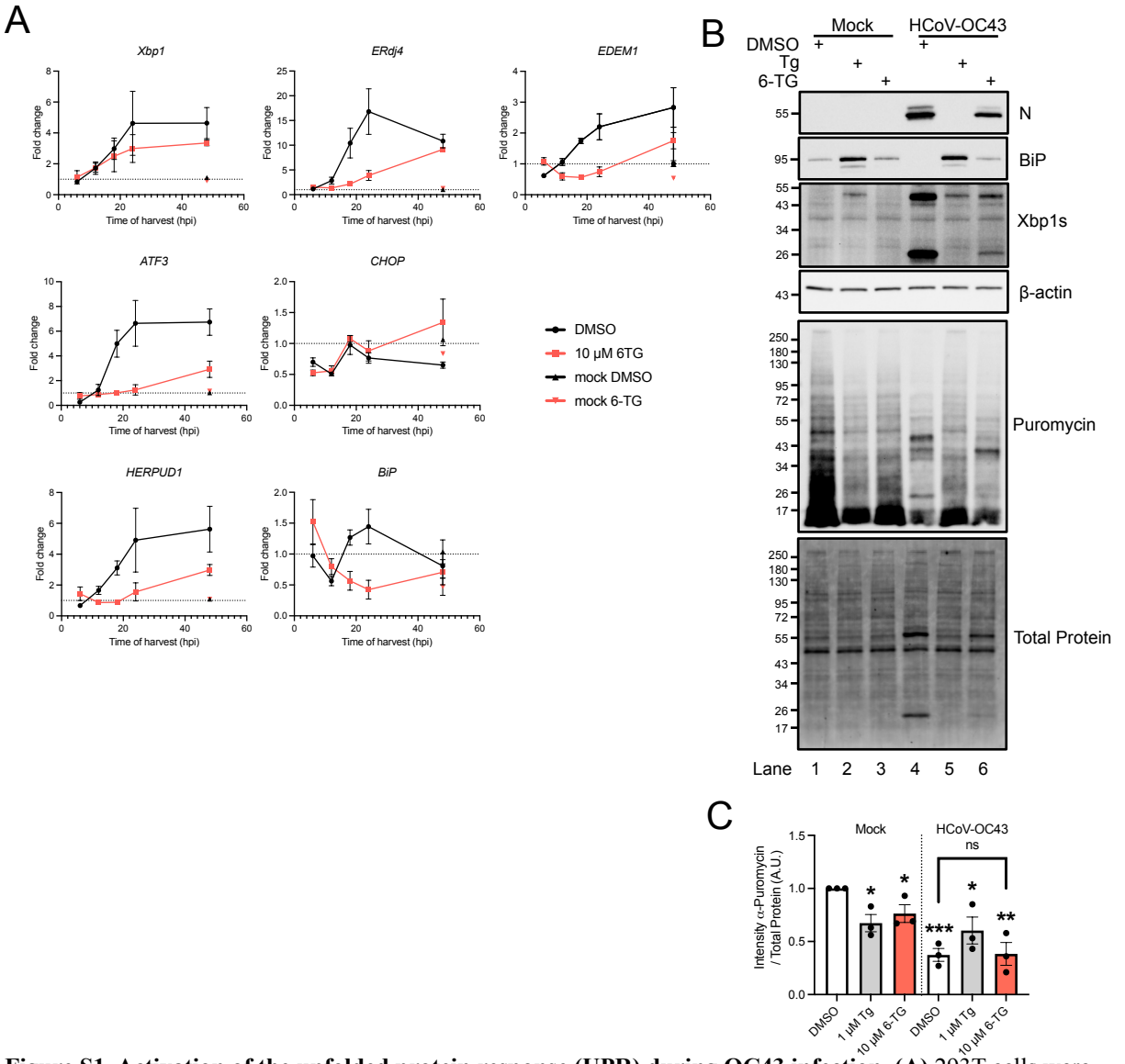

Figure S1. Activation of the unfolded protein response (UPR) during OC43 infection. (A) 293T cells were infected with HCoV-OC43 at an MOI of 0.1 then treated with 10 μM 6-TG or DMSO vehicle control. Total RNA from the cells were harvested at the times indicated and stored at -80°C until RT-qPCR analysis of UPR target genes. **(B)** 293A cells were infected as in (A), then treated with 10 μg 6-TG, 1μg thapsigargin (Tg), or DMSO. Cells were treated with 10 μg/mL of puromycin for 10 min prior to harvest 24 h after transfection. Lysates were probed by western blot as indicated. **(C)** Total puromycin intensity from (E) was quantified relative to total protein load and are graphed normalized to the mock-infected, DMSO-treated cells (n=3 ± SEM, statistical significance was determined by paired t-test compared to mock-infected, DMSO-treated cells; *, $p<0.05$; **, $p<0.01$; ***, $p<0.001$; ns, non-significant).

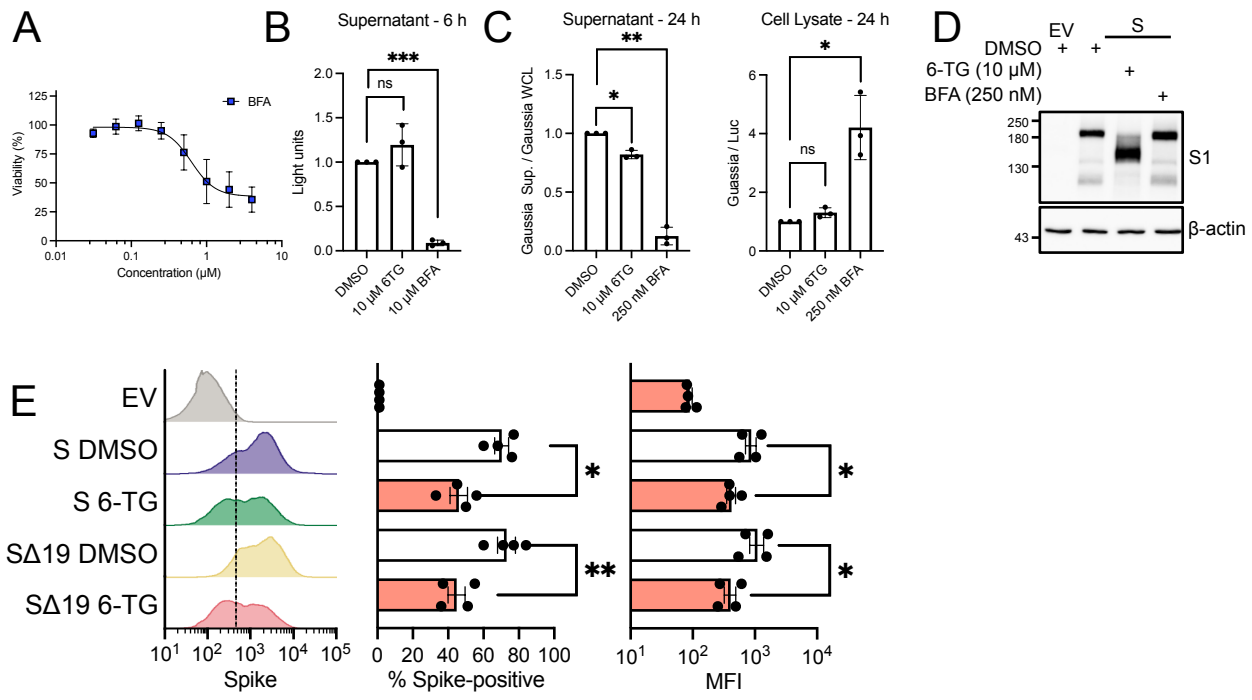

Figure S2. 6-TG reduces surface expression of Spike but does not globally limit secretion. (A) Alamar Blue cell viability assay of 293T cells treated with Bafilomycin A (BFA) (n=4±SEM). **(B)** 293T cells were transfected with *Gaussia* luciferase for 18 h then treated with 6-TG, BFA or DMSO vehicle control for 6 h . Supernatants were recovered from the cells and measured for luciferase activity. **(C)** 293T cells were transfected with both luciferase and *Gaussia* luciferase then treated with 6-TG, BFA, or DMSO. After 24 h, supernatants were removed and analyzed as in (B). Cell lysate was harvested in Reporter Lysis Buffer and stored at -80°C until both luciferase and *Gaussia* luciferase activity was measured. (For B and C, n=3 ± SEM, statistical significance was determined by paired t-test compared to DMSO-treated cells; *, $p<0.05$; **, $p<0.01$; ***, $p<0.001$; ns, non-significant). **(D)** 293T cells were transfected with SARS-CoV-2 Spike or EV then treated with 6-TG, BFA, or DMSO. Lysates were harvested 24 h after transfection in 2x Leammli buffer and were probed by western blotting as indicated. **(E)** 293T cells were co-transfected with EGFP and either Spike (S), Spike with 19 residue C-terminal truncation (SΔ19), or EV and then treated with 10 μM 6-TG or DMSO. After 24 h, cells were harvested, surface-stained for Spike then fixed prior to analysis by flow cytometry. EGFP+ cells were gated for analysis of number of Spike+ cells and Median Fluorescent Intensity (MFI) (n=4±SEM statistical significance was determined by paired t-test between 6-TG and DMSO treated cells; *, $p<0.05$).